

**Effects of Liquid-Gas Fraction on Vibrational Behaviour of
Piping System**

by

Nurul 'Awatif Hanani binti Hazarudin
22754

Dissertation submitted in partial fulfilment of
the requirements for the
Bachelor of Mechanical Engineering
With Honours

FYP II
January 2020

Universiti Teknologi PETRONAS
32610 Seri Iskandar
Perak Darul Ridzuan

CERTIFICATION OF APPROVAL

**Effects of Liquid-Gas Fraction on
Vibrational Behaviour Of Piping System**

by

Nurul 'Awatif Hanani Binti Hazarudin

22754

Dissertation submitted to the
Mechanical Engineering Programme
Universiti Teknologi PETRONAS
in partial fulfilment of the requirement for the
BACHELOR OF MECHANICAL ENGINEERING
WITH HONOURS

Approved by,



(Dr. Nabihah Sallih)

UNIVERSITI TEKNOLOGI PETRONAS
BANDAR SERI ISKANDAR, PERAK

January 2020

CERTIFICATION OF ORIGINALITY

This is to certify that I am responsible for the work submitted in this project, that the original work is my own except as specified in the references and acknowledgements, and that the original work contained herein have not been undertaken or done by unspecified sources or persons.



NURUL 'AWATIF HANANI BINTI HAZARUDIN

ABSTRACT

The two-phase flow of gas and liquids are normally found inside the oil and gas industry. The differences in properties and fractions of a two-phase flow mixture might cause vibration due to the variation of flow momentum. Excessive vibrations in piping systems might affect the safety of the plant and the integrity of the piping system. This phenomenon happens due to the excitation force that may exist by the different density and void fraction of gas inside the two-phase flow. This project presents a study on the vibration issue of the piping system due to the slug flow, which will be focusing on the effect of different liquid-gas void fraction onto the horizontal and vertical piping orientation and 90 elbow piping system. A set of six trials of three different void fractions and flow rate of 100 l/min and 200 l/min were used in this experiment. Analysis was done on the flow behavior at tee-junction and elbows to fully understand the causes and effects that it might have on the piping system. It is found that as there is a slight effect of increasing void fraction into the piping vibration.

ACKNOWLEDGEMENT

بِسْمِ اللَّهِ الرَّحْمَنِ الرَّحِيمِ

So, undoubtedly, along with the hardship there is ease. Undoubtedly, along with the hardship there is ease. [94: 5-6]

All praises to Allah, for all the knowledge, help and sustenance given.

This piece is dedicated to every person involved throughout this journey until the end.

Thank you for all the supports, guidance and prayers.

~'Awatif Hanani

Table of Contents

CHAPTER 1	1
INTRODUCTION	1
1.1 Background of study	1
1.2 Problem statement.....	3
1.3 Objective	4
1.4 Scope of study	4
CHAPTER 2	5
LITERATURE REVIEW	5
2.1 Flow in Piping	5
2.1.1 Types of flow.....	8
2.1.2 Orientation of Flow	11
2.1.3 Types of mixture.....	13
2.1.4 Mechanical Induced Vibration	16
2.2 Void fraction	17
2.3 Analytical and computational study	18
2.3 Highlights of Literature Review	23
CHAPTER 3	24
METHODOLOGY	24
3.1 Process Flow	24
3.2 Experimental set-up	25
3.3 Spectrum and time waveform analysis	28
3.4 Gantt Chart.....	29
3.5 Key Milestone	31
CHAPTER 4	32
RESULTS AND DISCUSSIONS	32
4.1 Characteristics of motor and pump	32
4.1.1 Spectrum vibration analysis.....	34
4.1.2 Time waveform vibration analysis	43
4.2. Effects of flow	49
4.2.1. Point 6 (Tee junction).....	50
4.2.2. Point 7 (Elbow 1).....	56
4.2.3. Point 8 (Elbow 2).....	60
CHAPTER 5	66
CONCLUSION AND RECOMMENDATION	66
REFERENCES	69

LIST OF FIGURES

- FIGURE 1.1. FCP Degassing boot piping system
- FIGURE 2.1. Baker's horizontal flow pattern map [10]
- FIGURE 2.2. The vertical flow regime transition according to Taitel et al. [10]
- FIGURE 2.3. A comparison study of Ishii and Mishima with Taitel et al. on the vertical flow pattern [10]
- FIGURE 2.4. The slug flow geometry [8].
- FIGURE 3.1. FYP Project Process Flow
- FIGURE 3.2. Tee junction (Point 6)
- FIGURE 3.3. Elbow (Point 7)
- FIGURE 3.4. Elbow (Point 8)
- FIGURE 3.3. FYP1 Gantt Chart
- FIGURE 3.4. FYP2 Gantt Chart
- FIGURE 4.3. Graph of axial motor spectrum for overall flow conditions (a) driven end (DE) (b) Non-driven end (NDE)
- FIGURE 4.4. Graph of vertical motor spectrum for overall flow (a) driven end (DE) (b) Non-driven end (NDE)
- FIGURE 4.5. Graph of horizontal motor spectrum for overall flow (a) driven end (DE) (b) Non-driven end (NDE)
- FIGURE 4.6. Graph of axial pump spectrum for overall flow (a) driven end (DE) (b) Non-driven end (NDE)
- FIGURE 4.7. Graph of vertical pump spectrum for overall flow (a) driven end (DE) (b) Non-driven end (NDE)
- FIGURE 4.8. Graph of horizontal pump spectrum for overall flow (a) driven end (DE) (b) Non-driven end (NDE)
- FIGURE 4.9. Graph of axial motor waveform (a) driven end (DE) (b) Non-driven end (NDE)
- FIGURE 4.10. Graph of horizontal motor waveform (a) driven end (DE) (b) Non-driven end (NDE)
- FIGURE 4.11. Graph of vertical motor waveform (a) driven end (DE) (b) Non-driven end (NDE)
- FIGURE 4.12. Graph of axial pump waveform (a) driven end (DE) (b) Non-driven end (NDE)

FIGURE 4.13. Graph of horizontal pump waveform (a) driven end (DE) (b) Non-driven end (NDE)

FIGURE 4.14 Graph of vertical pump waveform (a) driven end (DE) (b) Non-driven end (NDE)

FIGURE 4.15. Tee junction (Point 6)

FIGURE 4.16. Graph of all flow conditions (a) Point 6x (b) Point 6y (c) Point 6z

FIGURE 4.17. Graph time waveform of all flow conditions (a) Point 6x (b) Point 6y (c) Point 6z

FIGURE 4.18. Bubble formation at tee-junction (Point 6) for different void fraction of (a) Trial 3 ($\beta = 25\%$, $Q_1 = 0.0017 \text{ m}^3/\text{s}$) (b) Trial 5 ($\beta = 50\%$, $Q_1 = 0.0017 \text{ m}^3/\text{s}$) (c) Trial 4 ($\beta = 25\%$, $Q_1 = 0.0033 \text{ m}^3/\text{s}$) (d) Trial 6 ($\beta = 50\%$, $Q_1 = 0.0033 \text{ m}^3/\text{s}$)

FIGURE 4.19. Elbow (Point 7)

FIGURE 4.20. Graph of all flow conditions (a) Point 7x (b) Point 7y (c) Point 7z

FIGURE 4.21. Graph time waveform of all flow conditions (a) Point 7x (b) Point 7y (c) Point 7z

FIGURE 4.22. Elbow (Point 8)

FIGURE 4.23. Graph of all flow conditions (a) Point 8x (b) Point 8y (c) Point 8z

FIGURE 4.24. Graph time waveform of all flow conditions (a) Point 8x (b) Point 8y (c) Point 8z

FIGURE 5.1. Slug flow formation at tee-junction (Point 6) for different void fraction of (a) Trial 3 ($\beta = 25\%$, $Q_1 = 0.0017 \text{ m}^3/\text{s}$) (b) Trial 5 ($\beta = 50\%$, $Q_1 = 0.0017 \text{ m}^3/\text{s}$)

LIST OF TABLES

TABLE 2.1. Void fraction correlations-homogeneous-model-based correlations [24]

TABLE 2.2. Void fraction correlations of slip-ratio [24]

TABLE 2.3. Void fraction correlations of drift-flux-model-based [24]

TABLE 3.1. Experimental data

TABLE 3.2. Project Key Milestones

TABLE 4.1. Characteristic of the motor

TABLE 4.2. Axial motor spectrum

TABLE 4.3. Vertical motor spectrum

TABLE 4.4. Horizontal motor spectrum

TABLE 4.5. Axial pump spectrum

TABLE 4.6. Vertical pump spectrum

TABLE 4.7. Horizontal pump spectrum

TABLE 4.8. Spectrum point 6

TABLE 4.9. Spectrum point 7

TABLE 4.10. Spectrum point 8

CHAPTER 1

INTRODUCTION

1.1 Background of study

Fluid conveying pipes had been commonly used in various domestic and industrial fields especially in the oil and gas industry. They usually work almost non-stop every day to ensure enough supply could be channel at the end of the day. The inherent corrosive nature of many transported fluids and also due to the environment had often cause the defect of piping system. Apart from that, major threats to structural integrity of piping system such as the loss of strength, stiffness and vibration could also potentially cause damage to the piping system. Excessive vibrations in piping systems might affected the safety of plant and integrity of piping system [1-3]. It also could cause major problems such as downtime of machine, piping leakage, fatigue failures and even explosions in refineries and petrochemical plants [4]. There are various piping vibration issues that happens inside the oil and gas industry. Some of the root causes for the occurrence of high vibration inside piping system are:

- (1) The excitation of the mechanical natural frequency of piping system due to pulsation or any mechanical source [4]
- (2) Fluid-structure interaction, turbulent flow fluctuations and unsteady pressure [5]
- (3) Inadequate and weak piping support [5]

In this project, study had been done on the high vibration issue of Degassing Boot piping system at Garaff First Commercial Production Facilities (FCP), Iraq as shown in Figure 1.1. The verification had lead to the assumptions of the vibration pattern of piping system might be due to the combination of slug loading and Fluid Induced

Vibration (FIV). The finding from the as-built analysis is that at present, the system minimum natural frequency is at 0.579 Hz, which is under the minimum required value of 15 Hz for FIV case. Further study and analysis are required to really identify the vibration causes and effects on the piping system.

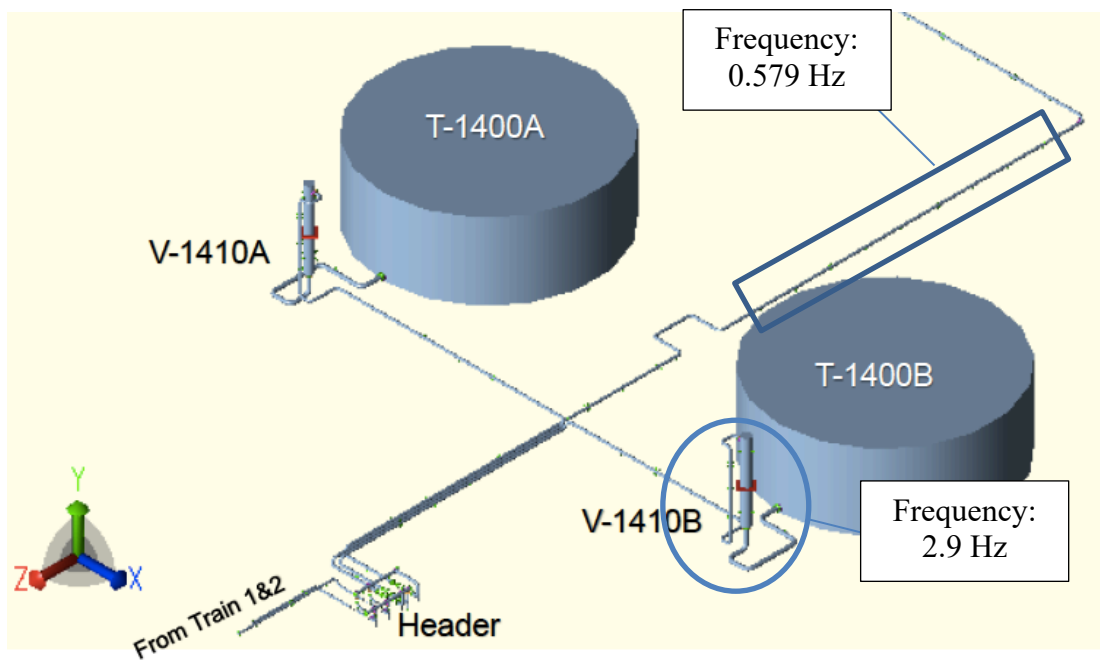


FIGURE 1.1. FCP Degassing boot piping system

1.2 Problem statement

The production of unconventional oil resources such as heavy oil, extra heavy oil, oil sand and bitumen are some of the available oil reserves remaining in the world. These products have gained more attention during recent years due to the increasing world energy demand [6]. During the oil production and transportation, the flow of crude is included with other elements such as water and gas. This condition is usually encountered in the oil wells, piping system and also during the production of oil. However, the physical nature of the crude oil itself (eg: high viscosity of crude) had make their production and transportation harder.

Since it is hard to control and predict the production consistency of these element present inside the piping system, it might be hard to know the flow patterns, liquid hold up and behaviour that these liquid might have throughout the whole production and transportation process due to their different properties. The two-phase flow vibration excitation mechanism is nearly identified to the variation of flow momentum due to the presence of different densities in phases [7]. Furthermore, these differences on the properties and fraction of two-phase flow mixture might cause vibration such as FIV due to the slug flow behaviour. Slug flow is one of the most frequent and unwanted flow behaviour that occurs in the production and transportation of hydrocarbon. The understanding and early prediction of slug flow is essential in the safety design of piping system, as the unpredictability of these flow pattern might increase the risk for accidents such as flooding and severe pipe corrosion [8].

FIV cases had been given more focus in the engineering fields especially the processing plant and piping system. It is important to really understand the subject matter as the knowledge of gas-liquid or two-phase flow could help in designing and ensuring the safety of operating systems. Besides, avoiding it from happening could reduce the occurrence of danger and property damage. For example, in 1974, a petrochemical plant had to bear the the property damage loss of \$114,000,000 for the explosion occurred due to one piping failure [4]. A good understanding of the vibration

problem could also help to increase the asset integrity thus, at the same time reducing the maintenance and operational cost value.

The phase fraction of two-phase flow (either gas-liquid or liquid-gas) could help to determine the phase distribution of flow throughout the piping system. Thus, helping to identify the flow behaviour that might occur at different fraction of liquid inside the pipeline. As this local phase distribution mechanism, which are strongly related with the interfacial structure and movement have yet to be known [9], study on the FIV effects on pipeline could help to foresee the effects that it might produce and at the same time, investigate method that can be used to reduce it.

1.3 Objective

The objective of this study is to investigate the effects of Liquid-Gas Fractions on the vibrational behaviour of piping system.

1.4 Scope of study

This project focuses on the behaviour of liquid-gas two-phase flow of water and gas. Apart from that, this project discusses the effect and relationship of different liquid-gas fractions with various velocity on the piping system. The flow would be focusing on the different orientations of tee-junction and 90° elbow pipe.

CHAPTER 2

LITERATURE REVIEW

This chapter describes related former work and study that had been done by researches on the flow in pipings, types of flow, types of mixture, void fraction, effect of behaviour on pipeline vibration and their method study. Besides, this chapter also shows the highlights of the project.

2.1 Flow in Piping

Piping had been used as the main transporting medium of fluid in oil and gas industries. The flow fields inside the systems are complex and usually include multiphase flow, consisting of different type of phases such as either gas-liquid or liquid-liquid phase flow. It is important to grasp the knowledge on variation of pattern produced in this phase flow as they have different particular property which may be suitable or not during processing or operation of system [10]. Numerous studies had been conducted to understand and study the regimes that might be produced during this two-phase flow [8, 10, 11]. Suitable flow patterns that could produce less pressure drop during the transportation of crude in the pipeline could be identify by knowing the two-phase flow regimes.

Baker was one of the first people to identify the flow regime based on his observation on concurrent flow of gaseous and condensate crude products inside a horizontal piping. During his study, he introduced the significance of flow pattern for the computation of pressure drop, heat transfer and mass transfer in tubes [8]. Thus, producing a flow pattern map known as Baker's horizontal flow pattern map [10]. The map was constructed using two parameters groups, G_1 , $\lambda\phi/G_g$ and G_g/λ .

These parameters are defined in terms of the liquid and vapor mass flux as expressed in Equations 2.1 and 2.2:

$$G_l = \frac{\dot{m}_l}{(A\rho_l)} \quad (2.1)$$

$$G_g = \frac{\dot{m}_g}{(A\rho_g)} \quad (2.2)$$

The dimensionless parameters of correction factor in Equation 2.3 and 2.4 to correlate the data and demonstrate Baker's chart, as shown in Figure 2.1.1:

$$\lambda = \left(\frac{\rho_g}{\rho_{go}} \frac{\rho_l}{\rho_{lo}} \right)^{0.5} \quad (2.3)$$

$$\phi = \left(\frac{\sigma_o}{\sigma} \right) \left[\frac{\mu_l}{\mu_{lo}} \left(\frac{\rho_{lo}}{\rho_l} \right)^2 \right]^{1/3} \quad (2.4)$$

\dot{m}_l : The flow rate of liquid mass

\dot{m}_g : The flow rate of gas mass

ρ_l : The density of liquid (kg/m³)

ρ_g : The density of gas (kg/m³)

ρ_{go} : The air density (at one atmospheric pressure and room temperature) (kg/m³)

ρ_{lo} : The water density (at one atmospheric pressure and room temperature) (kg/m³)

σ : Surface tension

σ_o : Surface tension of water

μ_l : The viscosity of liquid

μ_{lo} : The viscosity of water (at 1 atmospheric pressure and room temperature)

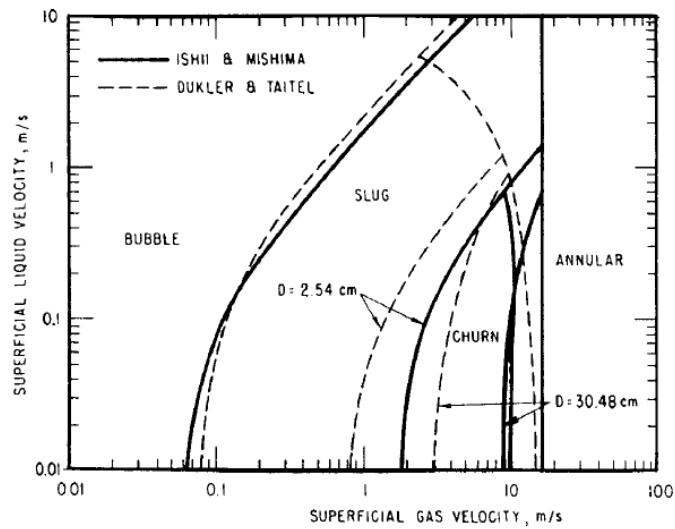


FIGURE 2.3. A comparison study of Ishii and Mishima with Taitel et al. on the vertical flow pattern [10]

The following sub-section describes the types of flow, orientation of the flow and types of mixture.

2.1.1 Types of flow

The flow regimes inside Baker's Chart could help in determining the type of flow inside the piping system. The Baker's chart horizontal flow map could be used for any combination of gas-liquid flow and it describes seven different flow regimes mentioned as [8]:

- (1) Stratified flow: It is a condition when the two phases is separated completely at low liquid and gas velocities
- (2) Wavy flow: It is a condition when waves which travel in the flow direction are formed on interface of liquid-gas due to an increase of gas velocity under stratified flow conditions.
- (3) Plug flow: It is a condition when flow forms an irregular flow pattern at low gas flow rates and moderate liquid rates. The liquid plugs are separated by zones of elongated gas bubbles where the diameter of elongated bubbles are separated by zones and the diameter is smaller than tube diameter. At

the end, a continuous liquid phase will be formed at the tube bottom underneath the bubbles.

- (4) Slug flow: It is a condition where liquid slugs become more chaotic than plug flow as the gas velocity increases.
- (5) Annular flow: It is a condition due to the formation of continuous film around the perimeter of tube. It is caused by an increment in gas flow rates. The gas velocity is the important factor in determining the thickness variation of film at the bottom and top of the tube.
- (6) Bubble flow: It is a condition when dispersion of gas bubbles in the continuous liquid flow occurs
- (7) Spray flow: It is a condition when dispersion of distinct liquid droplets happens in the continuous gas phase

On the other hand, the flow pattern in vertical direction that could be observed is bubble flow, plug/Taylor bubble flow and slug flow.

Another study by Miwa et al. [11] agreed that slug and churn flow regimes have the highest fluctuations when being compared to others. Structural vibration tends to exist in this condition due to the major differences in momentum of slug unit when flowing through the pipe. The presence of slug or churn flow conditions could also cause Fluid Induced Vibration (FIV) even when the flow regime was designed or set to stable annular flow. Rahbar et al. [8] used the CFD simulation with VOF model and compared the results with the Baker chart to predict the flow pattern of an inclined pipeline [8]. CFD is one of the normally used tool in analysing the multiphase flow [8]. The slug flow characteristic is determine inside the study by looking at the crucial parameters of slug flow such as the slug frequency, slug translational velocity, the hold up and pressure drop. The parameters could be determine by referring to Figure 2.4.

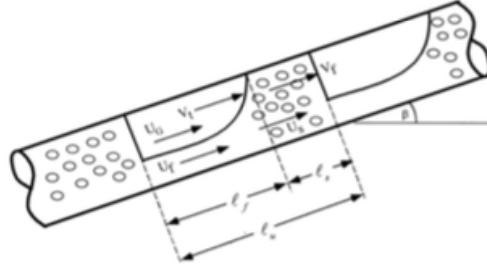


FIGURE 2.4. The slug flow geometry [8].

(a) Slug transitional velocity

Slug transitional velocity is the velocity interface between liquid slug and gas pocket. In Rahbar et al. [8] study, the slug transitional velocity is investigated in horizontal and downward inclined pipelines. It can be determined by using the Equations 2.5 until 2.7.

$$V_t = C_o V_m + V_d \quad (2.5)$$

$$V_d = 0.54\sqrt{gD}\cos\beta + 0.35\sqrt{gD}\sin\beta \quad (2.6)$$

$$V_m = V_{SL} + V_{Sg} \quad (2.7)$$

Where,

V_d : The drift velocity of elongated bubble (in a still liquid)

V_m : The velocity of mixture

V_{SL} : The summation of liquid

V_{Sg} : The velocity of gas superficial

C_o : The ratio of maximum velocity to mean velocity of fully developed velocity profile (1.2 indicates fully developed turbulent flow and 2.0 indicates fully developed laminar flow)

D : Pipe diameter

β : inclination angle measured from horizontal axis

g : acceleration of gravity

Meanwhile, for the slug velocities below 15 ms^{-1} , another empirical formula could be used as expressed in Equation 2.8.

$$V_t = 1.21(0.1134 + 0.94V_{SL} + V_{Sg}) \quad (2.8)$$

V_{LS} : Liquid flow rate or Superficial Velocity

(b) Slug Frequency, F_s

Slug frequency could be defined as the total number of slugs going by a specific point along the pipeline at a certain period of time. It could be determine by using Equation 2.9.

$$F_s = 0.0226 \left[\frac{V_{SL}}{gD} \left(\frac{212.6}{V_m} + V_m \right) \right]^{1.2} [0.836 + 2.75 \sin^{0.25}(\beta)] \quad (2.9)$$

Furthermore, the momentum occurred during the production of elongated bubbles in the fluids inside the piping systems could also produce a powerful vibration and mechanical force on the pipeline. This phenomena due to the transition flow to slug flow could leads to vibration and structural issues that might causes cracking and at the same time making the corrosion rates in the pipe increase [12]. Besides, FIV could also be produced due to the flow changes of the steady operating condition of ideal pipeline design of an actual operating conditions, which varies depending on the capacity or performance changes and improvement during operation [1].

2.1.2 Orientation of Flow

The force of liquid slug against the piping wall of different orientations produced large impact such that it resemble the water-hammer-like phenomena [11]. The physical aspects that might lead to the FIV in slug flow regimes are the relation of the frequency of momentum fluctuations with the natural frequency of piping and also the collision of liquid slug onto the structural surface that convey a large excitation force onto the structure. The fluctuating nature and excitation forces acting on the piping system

which varies vertical, horizontal, inclined or turning element will then induces vibration.

According to the study done by Rouhani et al. [10], for the flow in horizontal piping orientation, the co-current flow of liquid and gas would produce a non-symmetrical pattern which is affected by the consequence of gravity and liquid density. This condition generates stratification in vertical direction as the liquid flow would have high tendency to occupy the bottom piping, which will then forcing the gas to stay at the upper parts. In the meantime, other different forces such as surface tension, viscosity and other related body forces is also subjected to the liquid flow. As being shown in the Figure 2.5, the flow regimes of liquid-gas at horizontal piping orientation varies from stratified smooth flow to dispersed bubble flow. Each condition are observed at different situation and will produce different type of flow.

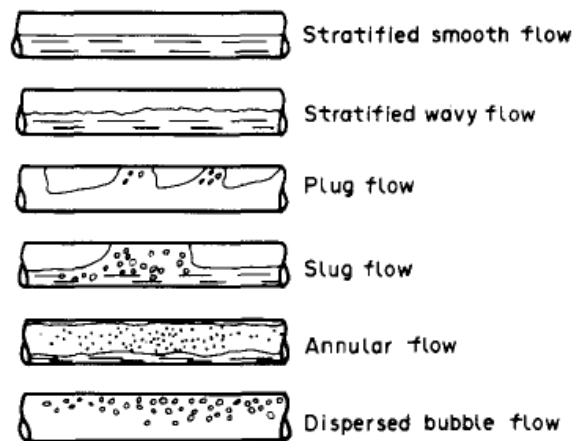


FIGURE 2.5. The schematics of horizontal orientation flow pattern

Meanwhile, flow in vertical piping orientation produces not much differences from the horizontal orientation. Vertical orientation two-phase flow pattern are much more axy-symmetrical because the gravity is being parallel to the flow direction. The flow regimes of vertical orientation would be as shown in Figure 2.6.

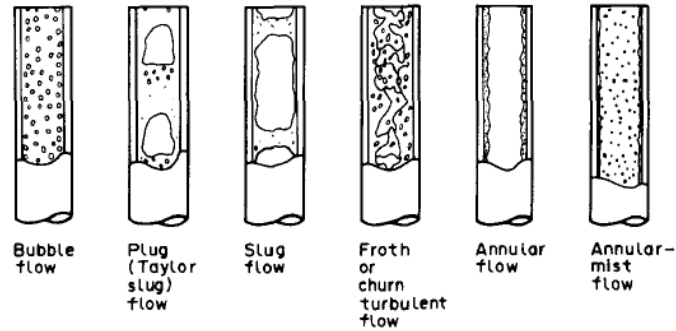


FIGURE 2.6. Schematics of vertical orientation flow pattern

For the flow across 90° elbow, Miwa et al. [11] mentioned in their study that a sharp-turning elbow section should be refrained in piping system so that collision effect due to impact force could be remove. Meanwhile, Gama [7] had also stated that the two-phase flow dynamic forces acting onto the piping elements such as bends and elbows may exert high level vibration [7]. According to the study done by Zhang et al. [13], fluids flow through a sharp elbow is a very complicated phenomenon due to the existence of large pressure gradient inside the region of the inside and outside of an elbow. An unbalanced force produces from the high velocity of fluid near the inside of an elbow and low velocity at the outside of an elbow produces a secondary flow field downstream of the elbow. Besides, this huge pressure gradient will generates vertices in flow. The presence of vertices inside the flow will increases the turbulence levels and causes structural vibration and flow-induced noise to occur.

2.1.3 Types of mixture

This section includes the discussion on the type of flow mixture inside the piping which exist either in single-phase, two-phase flow or multiphase flow. Multiphase flows are normally found in the oil and gas industries due to the presence of different element inside the piping system such as crude oil, water and even gas. Fluid flow is determined by the phase present, which is a discrete and homogeneous part of a system that is mechanically separable from the others [14].

(a) Single-phase

According to Evans [14] in his study, single-phase fluid flow is the existence of only one phase of matters, either liquid or gas. Even though it may include several different components in the same phase, it will only refer to the flow of liquid or gas. Single phase flow inside a circular pipe produces a thin layer of fluid against the pipe wall. This layer is known as boundary layer and the flow is retarded by friction. The increasing flow velocity will increase the boundary layer. The velocity distribution across this pipe is parabolic at laminar flow. For the single-phase fluid conditions, the velocity could be assume as laminar or turbulent flow by looking at the stable flow profile. Turbulent flow could exist due to the chaotic motion of fluid, which will then generates disturbances of flow in the form of vortices or eddies.

(b) Two-phase

Since the study of single-phase flow is simpler and still very much at the development stage, there are less information existed on the study of two-phase flow induced vibration due to its complexity [15]. The two-phase flow is the simultaneous flow of two of any of the three distinct phases of solid, liquid, gas or any substances or combination of them [16]. The movement of these flow lead to the slug formation, which will then increasing the pressure drop and possibility if phase changes [8]. The unstable nature of this flow produces local fluctuation of phase fraction, density, velocity, pressure field and momentum flux. All of these create periodic forces on piping or structure surfaces and might causes structural vibration, which will then lead to component failures due to the fatigue and wear. At the same time, the characteristics of unstable flow could induces resonance due to the coincidence of predominant frequency with the piping system's natural frequency [11]. The two-phase flow consists of different matters such as the gas – liquid two-phase flow and the liquid-liquid two phase flow.

It is quite difficult to determine the flow patterns of liquid-liquid two-phase flow due to the diversity of oil properties and differences of oil-water viscosity ratio [17]. When this two-phase flow move simultaneously in a piping system, this two fluids will

distribute themselves accordingly, depend on their own physical properties and operating parameters [18]. The wall roughness and wettability characteristic of pipe materials could also affect the oil-water patterns. Meanwhile, according to the study done by Angeli and Hewitt [19], the amount of data available on the liquid-liquid flow patterns is quite hard to obtained compared to the gas-liquid flow pattern.

Yusuf et al. [18] concluded that even though there are many available literature studies on the flow pattern and pressure drop in horizontal oil-water flow, it is still hard to construct the generalized a flow pattern map as the researches had used different properties of fluids in various piping configurations and operating condition. Their study had identify and classify six (6) patterns of oil-water flow which are the stratified (stratified smooth, stratified wavy), bubbly, dual continuous, annular, dispersed oil in water ($D_{o/w}$) and dispersed water in oil ($D_{w/o}$) as shown in Figure 2.7.

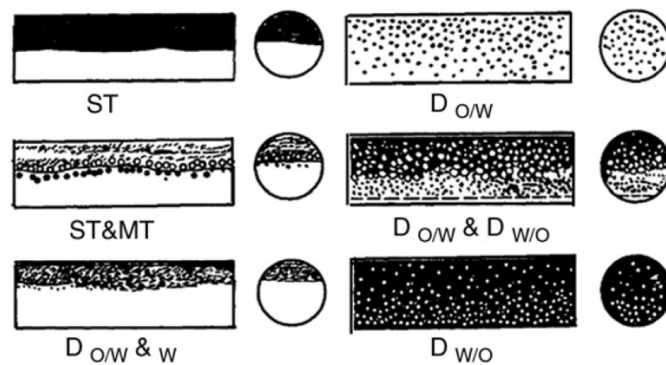


FIGURE 2.7. The oil - water flow patterns [17].

Meanwhile, the common source of pipe vibration is due to the internal two-phase flow of liquid and gas. This two-phase flow vibration excitation mechanism is also known to be related to the flow momentum variation due to the presence of phases with various densities [7].

A study had been done by Gama [7] to prove the feasibility of using pipe vibration response in order to evaluate the two-phase flow rates of liquid and gas. In this experiment, the two-phase flow conditions were determined by varying the air flow rate from 0.88 to 16.8 m³/h, the flow rate of water from 0.18 to 5.30 m³/h and the air

volume fraction from 50% to 95%. Based on the result, the flow conditions mostly correspond to the slug flow regime. Meanwhile, the vibration response during the experiment had shown that it is also depending on the pipe geometry, pipe material and boundary conditions. If the pipe natural frequency is in range of the excitation frequency of the two-phase flow band, a resonant behaviour is likewise expected to happen for some flow conditions. In determining the relationship between the pipe vibration and the two-phase flow, the root mean square (RMS) and the standard deviation were calculated from the acceleration data recorded. It could also be seen that the acceleration increase when the volume fraction of air is decreased. The piping vibration could also be reduced when the flow condition approaches the single phase. The highest level of vibration usually happens at the intermediated values of volume fraction. The study of different types of parameters and profiles such as the void-fraction profiles and bubble and liquid-velocity profiles are required to be able to interpret the two-phase flow [15].

In the study done by Miwa et al. [11], they had also proposed some of the recommendation to minimize the internal two-phase FIV. One of them is to fixed the piping structure's natural frequency to be much higher than the two-phase characteristic frequency of 0 to 50 Hz in order to avoid resonance mode. This could be done by adding solid supports against the piping wall or structure. Besides, the occurrence of the liquid slug should also be minimized.

2.1.4 Mechanical Induced Vibration

Besides from the effects of pulsation forces of flow inside the piping, there are other vibration excitation sources such as mechanical induced vibration. Wachel et. al [4] in their study had mentioned that mechanical excitation of machinery unbalanced forces and moments at one and two times the running speed is the next major excitation sources of piping vibration. The irregular flow through centrifugal machines such as pump and compressor generates fluid pulsations which having amplitudes corresponds to the multiples of the machines operating speed. The excitation produce high level and low frequency of pulsation.

2.2 Void fraction

Gama et al. [20] in their study stated that the two-phase flow vibration excitation mechanism have a close relation with the flow momentum variation from the differences that exist at the phases with different densities. It is crucial to know the two-phase volume fraction of phases to help determining the two-phase flow rates. Void fraction could be defined as the ratio of the volume occupied by the gas phase to the volume available for the flow [21].

Miwa et al. [11] confirmed that from the analytical and experimental studies done, it is shown that void fraction fluctuation effect is the most important part of two-phase analysis, regardless of the flow orientation. The highest force fluctuations were seen at the void fraction which corresponded to the slug or churn flow regimes. The phenomena happened due to the large intermittent change in mixture momentum flux due to the mixture fluid density. Thus, it could be clearly seen that the effect of flow regime, which is mainly related to the void fraction, has an exact effect on the excitation force. It is reported in this study that at high void fraction, there will be significantly high amplitude of surface waves in annular flow regime. Large momentum fluctuations will then be induced by the liquid slugs in the slug flow regime.

In another study done by Zhou et al. [22], it is mentioned that the void fractions is also highly related to the superficial velocity of liquid instead of the mass fractions ratio of the two-phases only. As also being stated by Riverin and Pettigrew [23], increasing velocity will make the characteristic size of bubbles and droplets to become smaller. When external force such as hydrodynamic force act on a structure or piping system, it induce destructive vibrations onto it which will then cause acoustic and noise problems. This phenomenon is also known as Fluid-Induced Vibration (FIV) [11]. The FIV terminology was proposed in 1977 by Robert Blevins which had classify the phenomenon into steady and unsteady conditions [11]. Excessive vibration could causes system failure and disrupt the operation of system. Furthermore, due to the highly unstable and unsteady nature of two-phase flow, local fluctuations of phase fraction, density, velocity, pressure and momentum flux is created.

2.3 Analytical and computational study

In predicting the FIV phenomena, separate models for fluid and structural dynamics can be built and coupled along with hydrodynamic and structural force terms [11]. However, since fluid dynamic model can be more difficult to study due to the nonlinear and multi-degree-of-freedom behaviours, the verification of model should always be done through experiment. Xue et al. [24] had classified the performances and correlations of different void fraction into three types which are: (1) Homogeneous-model-based correlation, (2) Slip-ratio-model-based correlation and (3) Drift-flux-model-based correlation. All these could help in predicting the void-fractions of the gas-liquid two-phase flows in different conditions.

The homogeneous-model-based could be assumed to happen during the fixed velocity of liquid-gas phase homogeneous mixture flow. The void fraction, α is considered as the function of the gas-liquid volumetric flow rate ratio, β such as shown in Equation 2.10. The value of β could be determined by Equation 2.11.

$$\alpha = f(\beta) \quad (2.10)$$

$$\beta = \frac{Q_G}{Q_G + Q_L} \quad (2.11)$$

Where, Q_g : the gas volumetric flow rate

Q_l : the liquid volumetric flow rate

Table 2.1 shows few correlations that can be obtained from the past studies. It can be seen that the void fraction is viewed as a linear function of the gas-liquid volumetric flow rate ratio, β . The slope coefficient of the equations is either constant or a function of some physical properties. However, the effect of the fluid velocities and physical properties of two phases on the void fraction are negligible.

TABLE 2.1. Void fraction correlations-homogeneous-model-based correlations [24]

References	Void fraction correlations
Armand (1946)	$\alpha = 0.833\beta$
Armand (1959)	$\alpha = (0.833 + 0.167x)\beta$
Nishino et al. (1963)	$\alpha = 1 - \left[\frac{1-x}{x} \frac{\rho_G}{\rho_L} \beta \right]^{0.5}$
Greskovich (1975)	$\alpha = \left[\left(1 + 0.671 \left(\frac{(\sin\theta)^{0.263}}{Fr^{0.5}} \right) \right) \right]^{-1} \beta$
Czop et al. (1994)	$\alpha = -0.285 + 1.097\beta$
Hajal et al. (2003)	$\alpha = \frac{\beta - \alpha_{ra}}{\ln(\beta/\alpha_{ra})}$ <p style="text-align: center;">Where</p> $\alpha_{ra} = \frac{x}{\rho_G} \left\{ [1 + 0.12(a-x)] \left[\frac{x}{\rho_G} + \frac{1-x}{\rho_L} \right] + \frac{1.18(1-x)g\sigma(\rho_L - \rho_G)^{0.25}}{G\rho_L^{0.5}} \right\}$

Meanwhile, slip-ratio-model-based correlations occurred during the condition where the gas and liquid phase travel separately with different velocities and one of the phase dispersed into the other uniformly. In this correlation, the value of void fraction, α is determined by equation 2.12.

$$\alpha = \frac{1}{1 + \left(\frac{1-x}{x}\right)\left(\frac{\rho_G}{\rho_L}\right) S_P} \quad (2.12)$$

Where, ρ_g : the gas density, kg/m³

ρ_L : the liquid density, kg/m³

The ratio could be defined by following Equation 2.13 or 2.14 and x could be determined by Equation 2.15. Equation 2.14 had been used frequently in previous studies to described the slip-ratio of two-phase flows. The differences correlations are shown in Table 2.2. Based on the past literatures, it could be concluded that this correlation can produced a better prediction capability of void fraction larger than 0.45.

$$S_P = \frac{u_G}{u_L} \quad (2.13)$$

$$S_p = A_s \left(\frac{1-x}{x}\right)^p \left(\frac{\rho_G}{\rho_L}\right)^q \left(\frac{\mu_L}{\mu_G}\right)^r \quad (2.14)$$

$$x = \frac{Q_G \cdot \rho_G}{Q_L \cdot \rho_G + Q_G \cdot \rho_G} \quad (2.15)$$

Where, ρ_G : the gas density, kg/m³

ρ_L : the liquid density, kg/m³

μ_G : the dynamic viscosity of gas, Pa.s

μ_L : the dynamic viscosity of liquid, Pa.s

A_s , p , q , r : coefficient

TABLE 2.2. Void fraction correlations of slip-ratio [24]

References	Values for:			
	A_s	p	q	r
Lockhart (1949)	0.28	-0.36	-0.64	0.07
Fauske (1961)	1	0	-0.5	0
Thom (1964)	1	0	-0.11	0.18
Zivi et al. (1964)	1	0	-0.33	0
Turner & Wallis (1965)	1	-0.28	-0.6	0.08
Baroczy (1966)	1	-0.26	-0.35	0.13
Smith (1969)	$\frac{0.4 + 0.6 \sqrt{\frac{\rho_L}{\rho_G} + 0.4 \left(\frac{1-x}{x}\right)}}{\sqrt{1 + 0.4 \left(\frac{1-x}{x}\right)}}$	0	1	0
Chisholm (1973)	$\sqrt{1 - x \left(1 - \frac{\rho_L}{\rho_G}\right)}$	0	1	0
Madsen (1975)	1	$\frac{\log\left(\frac{\rho_L}{\rho_G}\right)}{\log\left(\frac{1-x}{x}\right)}$	-1.5	0
Spedding & Chen (1984)	2.22	-0.35	-0.35	0

Chen (1986)	0.18	-0.4	-0.67	0.07
Hamersma et & Hart (1987)	0.26	-0.33	-0.67	0
Zhao et al. (2000)	$\alpha^{-0.125}$	-0.125	-0.126	0.875

The drift-flux-model-based correlations is established from the distribution parameter C_0 and the drift velocity U_{gm} such as shown in Equation 2.16. The correlations of this parameter from the previous studies done is shown in Table 2.3.

$$\langle\langle u_G \rangle\rangle = \frac{\langle J_G \rangle}{\alpha} = C_0 \langle J_m \rangle + \langle\langle U_{gm} \rangle\rangle \quad (2.16)$$

Where, $\langle \rangle$ or $\langle\langle \rangle\rangle$ are the area-averaged value and void-fraction-weighted mean value. The parameter of C_0 depends on the pressure, channel geometry and flow rate while U_{gm} could be correlated with parameters Π_1 and Π_2 defined by Equation 2.17 and 2.18.

$$\Pi_1 = \left(\frac{g\sigma(\rho_L - \rho_G)}{\rho_L^2} \right)^{0.25} \quad (2.17)$$

$$\Pi_2 = \left(\frac{gd_h(\rho_L - \rho_G)}{\rho_L^2} \right)^{0.5} \quad (2.18)$$

Where, ρ_g : the gas density, kg/m³

ρ_L : the liquid density, kg/m³

g : 9.81 m/s², gravitational acceleration (m/s²)

d_h : diameter of bubble (m)

σ : Surface tension coefficient (N/m)

TABLE 2.3. Void fraction correlations of drift-flux-model-based [24]

References	Distribution Parameter, C_0	Drift Velocity, U_{gm} (m/s)
Rouhani (1970)	$1 + 0.2(1-x)\left(\frac{gD\rho_L^2}{G^2}\right)^{0.25}$	$1.18\Pi_1$
Bonnecaze (1971)	1.2	$0.35\Pi_2$
Greskovich & Cooper (1975)	1	$0.71\sqrt{gD}(\sin\theta)^{0.263}$
Beattle (1986)	$1 + 2.6f_{tp}^{0.5}$	$0.35\Pi_2$

Hibiki & Ishii (2003) [24]	$1.2-0.2(\rho_G/\rho_L)^{0.5}(1 - \exp(-18\alpha))$	$1.414\Pi_1(1 - \alpha)^{1.75}$
Hibiki & Ishii (2003)	$1.2-0.2(\rho_G/\rho_L)^{0.5}$	$0.35\Pi_2$
Hibiki & Ishii (2003)	$\left(1 + \frac{\frac{1 - \alpha}{\alpha + 4\sqrt{\frac{\rho_G}{\rho_L}}}}{\sqrt{\frac{(\rho_L - \rho_G)gD(1 - \alpha)}{0.015\rho_G}}} + 1\right)$	$\left(\frac{\frac{1 - \alpha}{\alpha + 4\sqrt{\frac{\rho_G}{\rho_L}}}}{u_m + \sqrt{\frac{(\rho_L - \rho_G)gD(1 - \alpha)}{0.015\rho_G}}}\right)$

All these correlations are useful in determining the void fractions at different conditions where it could be observed that void fraction could be distributed into three different regions. However, one should take into consideration that majority of the correlations stated in Tables 2.1. until 2.3. have large errors when the void fraction of the two-phase flow is small.

Following that, a relation between pipe peak frequency and void fraction had been introduced by L.E. Ortiz-Vidal et al. [25] in their study. Flow-induced vibration studies demonstrated that different parameters such as fluid density and velocity might affect the peak frequency value of natural frequency. The fluid density of two-phase flow is highly depended on the void fraction. Due to that, equation 2.19 of the peak frequency of the i -th mode had been introduced by the author. The value of hydrodynamic mass, m_h and shear velocity, J could be computed by equation 2.20 and 2.21.

$$\omega_{peak-i} = (\lambda_i L_{span})^2 \sqrt{\frac{EI}{m_p L_{span}^4}} \cdot \left(\frac{m_p}{m_p + m_h}\right)^{1/2} \cdot \sqrt{1 - \zeta_T^2} \cdot \sqrt{1 - \frac{c_J m_h J^2}{EI(\lambda_i)^2}} \quad (2.19)$$

$$m_h = c_m \rho_L A (1 - \alpha) \quad (2.20)$$

$$J = \sqrt{\frac{\tau_w}{\rho_M}} \quad (2.21)$$

Where, $\lambda_i L_{span}$: the roots of frequency equation

L_{span} : Length of pipe

m_p : linear mass density of the pipe

m_h : hydrodynamic mass

ζ : damping

c_j : 0.55 (for first mode), 1 (for the others)

c_m : hydrodynamic mass coefficient (1 equal to proportional hydrodynamic mass to mixture density)

ρ_M : density of mixture (kg/m^3)

ρ_L : density of liquid (kg/m^3)

A : cross-sectional area of pipe (mm^2)

Experimental observations had also been done and compared with the analytical approach. Based on the results obtained, it can be concluded that the peak frequency of homogeneous void fraction will decrease with an increase in the velocity of the mixture. The void fractions and flow pattern also affected the structural and vibration response of the pipe system.

2.3 Highlights of Literature Review

Based on the literature review conducted, this study is done to fill in the available research gap of liquid and gas two-phase flow of the air and water by focusing on their relation with two-phase flow. Besides, most of the existing study had focused on either the vertical or horizontal orientation piping and flow across elbow only. Thus, this study is aimed to focus on studying the vibration effects on tee junction and elbow orientation piping due to the slug flow.

CHAPTER 3 METHODOLOGY

This chapter will be discussing on the process flow and methodology that is performed in this study.

3.1 Process Flow

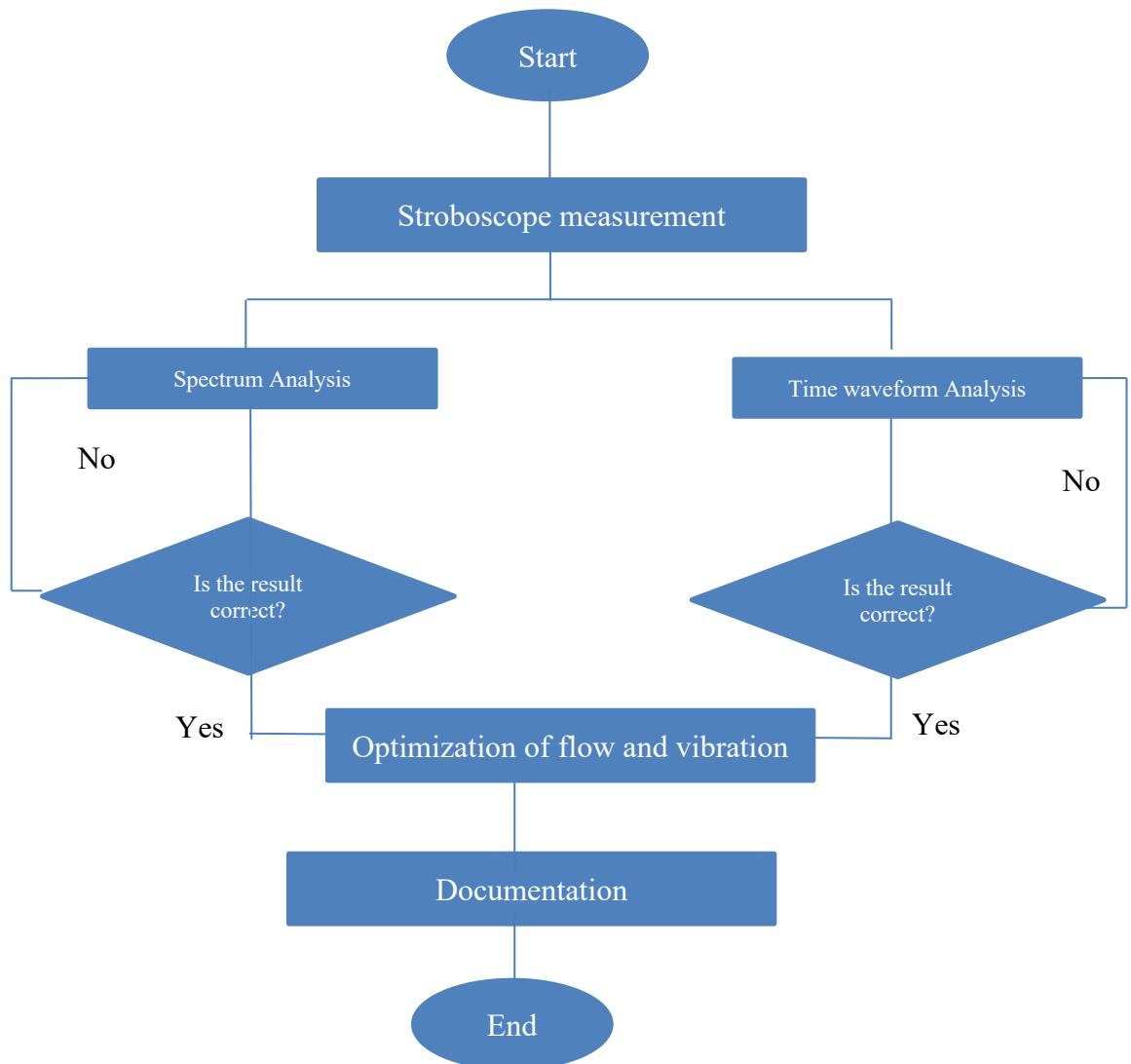


FIGURE 3.1. FYP Project Process Flow

3.2 Experimental set-up

In this project, a piping system with piping elements of a tee junction and two elbows is setup, with the valve opening left fully opened. Sensors are located at different measurement points. For the motor and pump, the sensors are located at the radial (vertical and horizontal) and axial planes of motor-pump non driven end (NDE) and motor-pump driven end (DE). Meanwhile, the sensors for point 6 at tee-junction are located in three different axis of x, y and z-axis such shown in figure 3.2 until 3.4 below. Vibration measurement for different flow conditions is taken using stroboscope and the data are recorded.

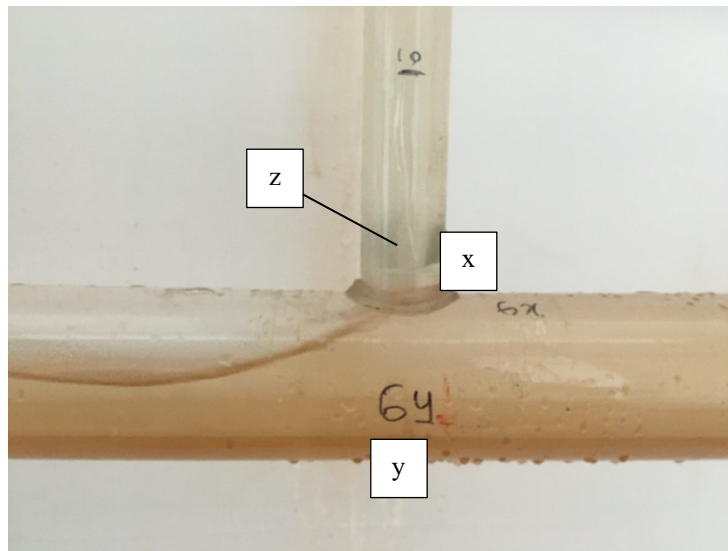


FIGURE 3.2. Tee junction (Point 6)

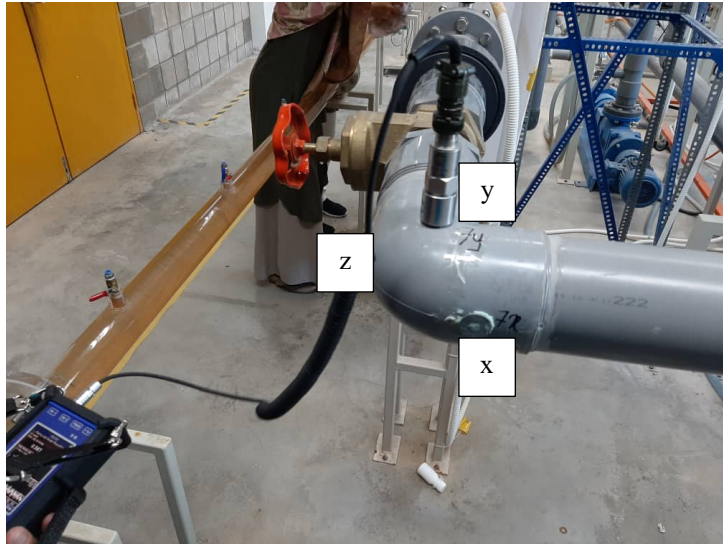


FIGURE 3.3. Elbow (Point 7)

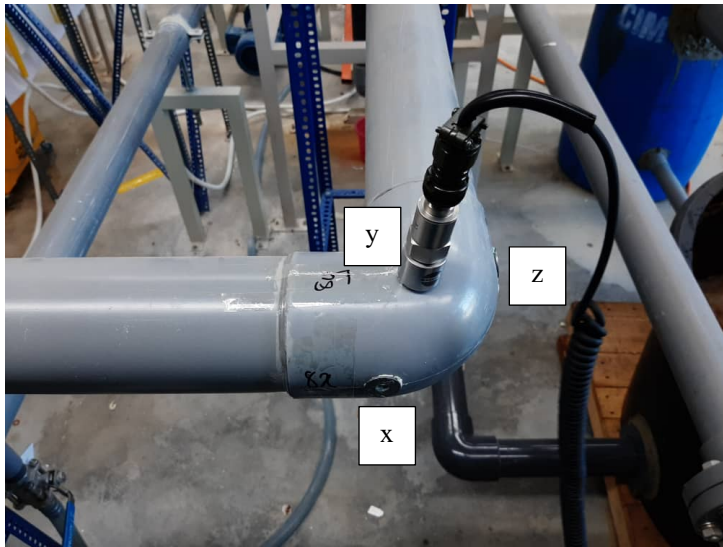


FIGURE 3.4. Elbow (Point 8)

The flow conditions used in the experiment are shown in Table 3.1. The flow conditions could be determined by looking at two parameters which are void fraction, β and superficial velocity, j such as shown in equations 3.1 until 3.2 [23]. A set of six trials of three different void fraction ($\beta = 0\%$, 25% and 50% and flow rate of 100 l/min and 200 l/min were used in this experiment. The void fraction is taken from the 19.25 cfm total air supplied. These trial conditions is then mapped back onto the flow regime map to know the type of flow pattern produced during each trials.

$$\beta = \frac{Q_g}{Q_g + Q_l} \quad (3.1)$$

$$j = \frac{Q_g + Q_l}{A} \quad (3.2)$$

Where,

A: total flow area

Q_g : Volumetric flow rate of gas, m³/s

Q_l : Volumetric flow rate of liquid, m³/s

The area of the piping system could be determined by using equation 3.3.

$$A = \pi r^2 \quad (3.3)$$

Where,

Pipe's circumference: 253 mm

Pipe's thickness: 3 mm

Internal diameter (ID): 74.53 mm

$$A_{pipe} = \pi(37.27)^2$$

$$\begin{aligned} A_{pipe} &= 4362.67 \text{ mm}^2 \\ &= 0.004363 \text{ m}^2 \end{aligned}$$

TABLE 3.1. Experimental data

Trial	Air		Water		Superficial velocity of air, j_g (m/s)	Superficial velocity of water, j_l (m/s)	Type of flow pattern
	β (%)	Volumetric flow rate, Q_g (m ³ /s)	Flowrate (l/min)	Volumetric flow rate, Q_l (m ³ /s)			
1	0	0	100	0.001667	0	0.3821	-
2	0	0	200	0.00333	0	0.7632	
3	25	0.002271	100	0.001667	0.521	0.3821	Slug flow
4	25	0.002271	200	0.00333	0.521	0.7632	Slug flow
5	50	0.004543	100	0.001667	1.041	0.3821	Slug flow
6	50	0.004543	200	0.00333	1.041	0.7632	Slug flow

3.3 Spectrum and time waveform analysis

Spectrum analysis enables the separation of components that overlap in the waveform and displayed it by frequency. This could help in determining the severity and source of the problem inside a system. It could be obtained by the derivation of waveform through the Fast Fourier Transform (FFT) process. FFT could help to separate the complex waveforms into a much simpler frequency graph.

Meanwhile, time waveform analysis enables one to see the combination of individual vibration signals inside a complex time waveform. It also could help to determine the overall vibration of the system. Time waveform should be used in complementary to the frequency spectrum for more wholistic vibration analysis. This is because some vibration characteristics such as impact or unbalance could be recognized more easily in time waveform by their high spikes and “M-W” peaks, relatively as these characteristics are not apparent in the frequency spectrum.

The vibration measurement obtained from the stroboscope measurement, will then be analysed by plotting the spectrum and time waveform graph in order to determine the vibration behavior of the piping system.

3.4 Gantt Chart

This section represent the planning for this whole project, represented in the gantt chart for the whole Final Year Project (FYP) 1 and 2. Figure 3.3. illustrates the gantt chart for FYP 1 and Figure 3.4. illustrates the gantt chart for FYP 2.

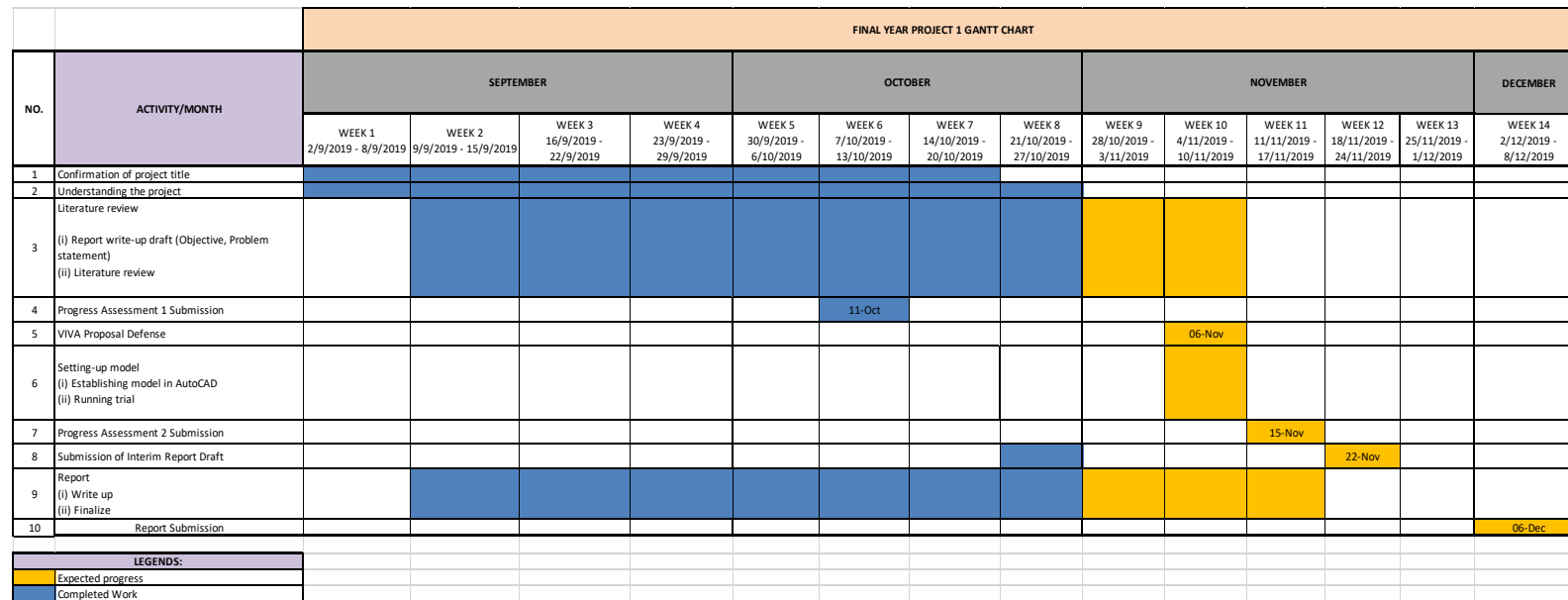


FIGURE 3.3. FYP1 Gantt Chart

		FINAL YEAR PROJECT 2 GANTT CHART													
NO.	ACTIVITY/MONTH	JANUARY				FEBRUARY				MARCH				APRIL	
		WEEK 1	WEEK 2	WEEK 3	WEEK 4	WEEK 5	WEEK 6	WEEK 7	WEEK 8	WEEK 9	WEEK 10	WEEK 11	WEEK 12	WEEK 13	WEEK 14
1	Experimental set-up			24-Jan											
2	Vibration reading (Stroboscope measurements)														
3	Data Analysis (Spectrum and Time Waveform)								05-Mar						
4	Progress Assessment 1 Submission						11-Feb								
5	Report Write-up														
6	Submission of draft dissertation								06-Mar						
7	Submission of dissertation (soft-bound)									13-Mar					
8	Viva presentation														
9	Progress Assessment 2 Submission														
10	Submission of project dissertation (hard bound)														18-Apr
LEGENDS:															
	Expected Progress														
	Completed Work														

FIGURE 3.4. FYP2 Gantt Chart

3.5 Key Milestone

The project planning key milestone is shown in Table 3.2.

TABLE 3.2. Project Key Milestones

No.	Key Activity	Date	Progress completion (%)
1	Submission of Progress Assessment 1	11/10/2019	5
2	VIVA Proposal Defense	6/11/2019	10
3	Submission of Progress Assessment 2	15/11/2019	15
4	Submission of Interim Report (Draft)	22/11/2019	20
5	Submission of report	6/12/2019	25
6	Experiment setup	24/1/2020	30
7	Vibration reading (Stroboscope measurement)	4/3/2020	40
8	Submission of Progress Assessment 1	11/2/2020	45
9	Data Analysis	5/3/2020	85
10	Submission of draft dissertation	6/3/2020	90
11	Dissertation submission (Soft-bound)	13/3/2020	0
12	Project dissertation submission (Hard-bound)	18/4/2020	0

CHAPTER 4

RESULTS AND DISCUSSIONS

This chapter presents the results and discussions in this study on the characteristic of motor and pump and also effects of flow.

4.1 Characteristics of motor and pump

In understanding the effects of the liquid-gas fraction on vibrational behavior of the piping system, it is necessary to look into the flow behavior at every point, motor-pump axis, spectrum vibration pattern and time waveform vibration pattern that they produced. All of these should be related to each other. As being mentioned by Wachel et. al [4] in their study, excitation from machinery unbalanced forces and moments or also known as mechanical induced could produce pulsation forces that could excite the vibration inside a piping system. Thus, it is better to firstly understand the characteristic of equipment such as motor and pump inside the system before analysing the effects that it might have onto the system.

The motor used inside this experiment is a 4 poles, 3-phase induction motor. As the coils inside the induction motor are energized, a rotating magnetic field exists inside the stator. The speed of the rotation depends on the number of coils or the number of “poles”. The speed would be 1500 RPM producing peak rated of 25 Hz ($1500\text{RPM}/60 = 25\text{Hz}$). However, stroboscope measurement taken inside the lab shows the actual peak rated of 24.5 Hz instead of the rated peak of 25 Hz probably due to the inefficiency of the motor. Table 4.1 below shows the characteristic of the motor.

TABLE 4.1. Characteristic of the motor

No.	Element motor - pump	Value
1	Speed motor	1500 RPM
2	Peak frequency (Rated)	25 Hz
3	Peak frequency (Actual)	24.5 Hz
3	Number of pole	4 poles (4 x 24.5 Hz = 98 Hz)



FIGURE 4.1. Description of the induction motor

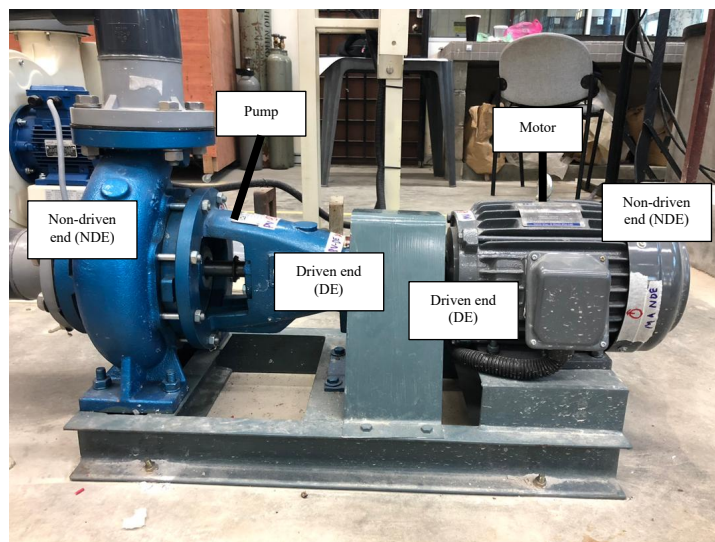


FIGURE 4.2. Motor and pump

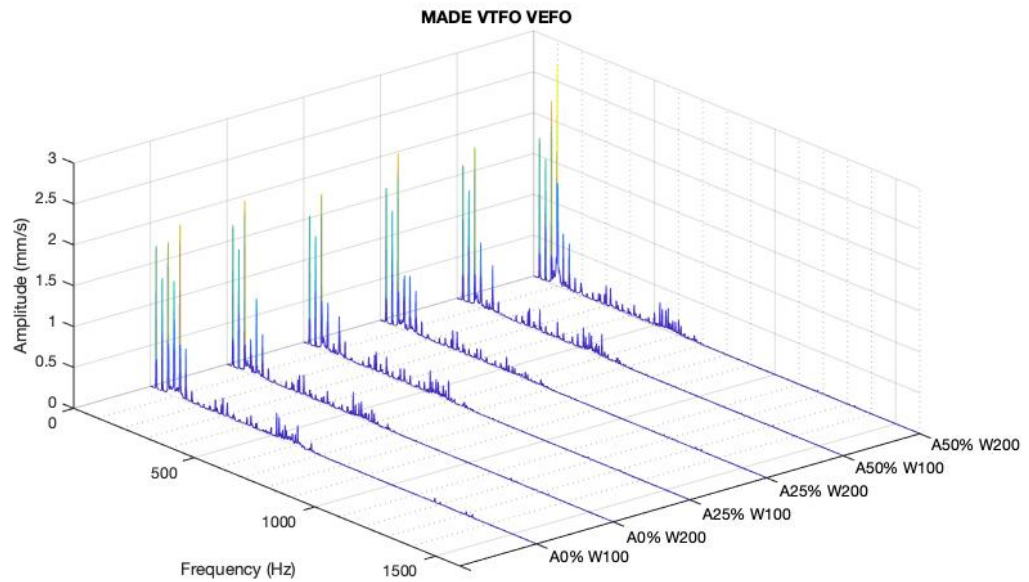
4.1.1 Spectrum vibration analysis

For the motor-pump, vibration measurement spectrum of different axis, which are axial, vertical and horizontal were taken. The spectrum results for motor are shown in Table 4.2 until Table 4.4 and Figure 4.3 until Figure 4.5. Meanwhile, the spectrum results for pump are shown in Table 4.5 until Table 4.7 and Figure 4.6 until Figure 4.8.

TABLE 4.2. Axial motor spectrum

Trial	DE		NDE	
	Max. Amplitude (mm/s)	Max. Frequency (Hz)	Max. Amplitude (mm/s)	Max. Frequency (Hz)
1	2.1248	123	1.8952	123
2	2.0911	73	2.1562	73
3	1.9034	73	1.8361	73
4	2.127	73	2.4496	73
5	1.934	73	1.7892	98
6	2.6947	73	2.331	73

(a)



(b)

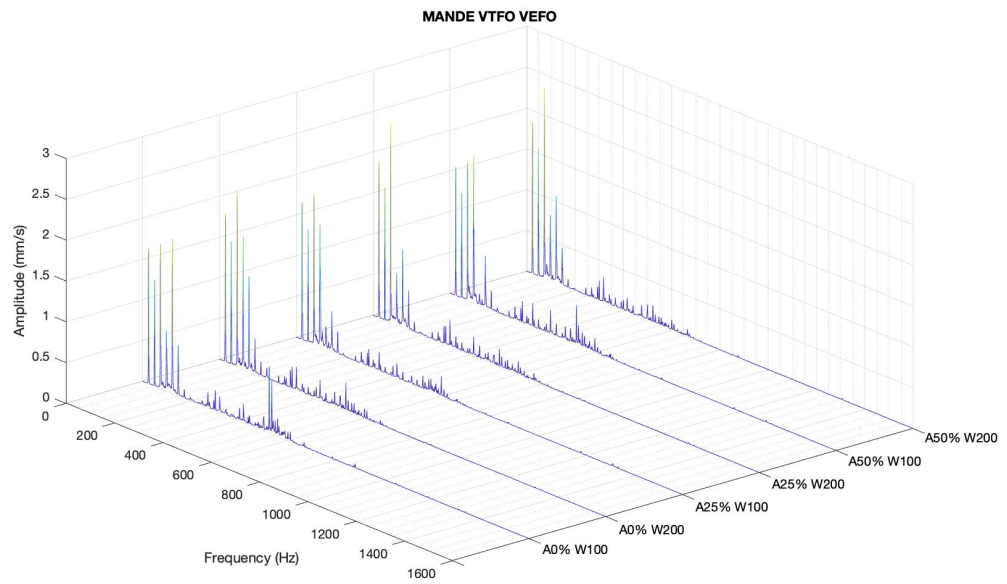
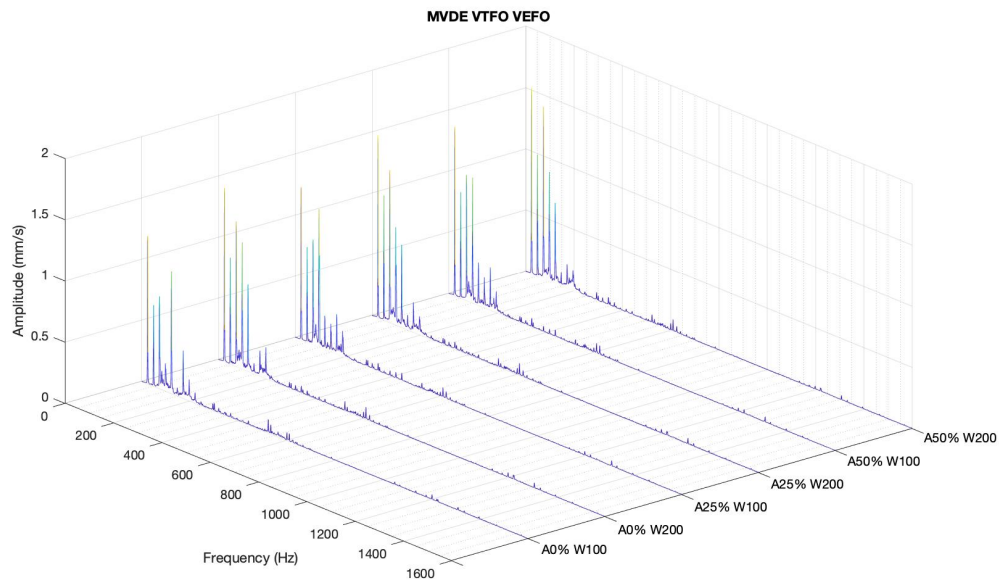


Figure 4.3. Graph of axial motor spectrum for overall flow conditions (a) driven end (DE) (b) Non-driven end (NDE)

TABLE 4.3. Vertical motor spectrum

Trial	NDE		DE	
	Max. Amplitude (mm/s)	Max. Frequency (Hz)	Max. Amplitude (mm/s)	Max. Frequency (Hz)
1	1.0767	98	1.2069	24 – 25
2	1.2051	98	1.4184	24 – 25
3	0.72582	98	1.246	24
4	1.1939	98	1.4893	24
5	1.7096	98	1.3792	24
6	1.05353	73	1.5177	24

(a)



(b)

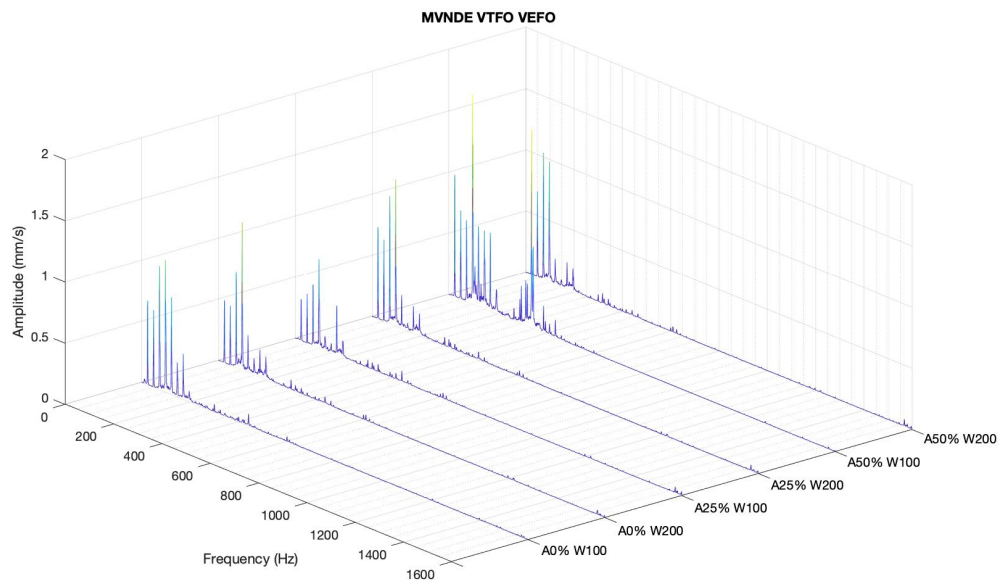
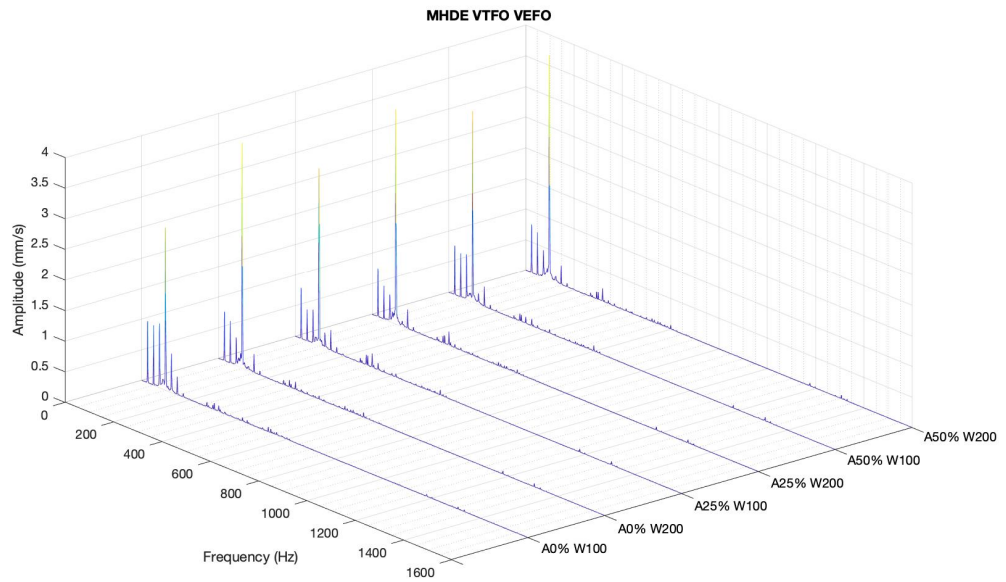


Figure 4.4. Graph of vertical motor spectrum for overall flow (a) driven end (DE)
(b) Non-driven end (NDE)

TABLE 4.4. Horizontal motor spectrum

Trial	NDE		DE	
	Max. Amplitude (mm/s)	Max. Frequency (Hz)	Max. Amplitude (mm/s)	Max. Frequency (Hz)
1	3.1327	98	2.6535	98
2	3.1821	98	3.6768	98
3	2.3946	98	2.9015	98
4	3.6874	98	3.5084	98
5	3.2651	98	3.1155	98
6	3.8629	98	3.6668	98

(a)



(b)

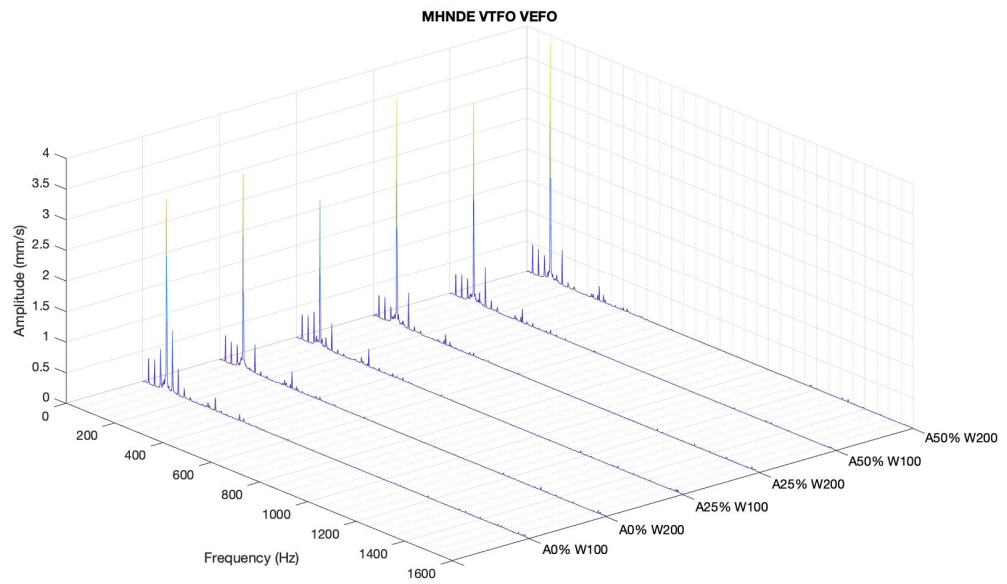
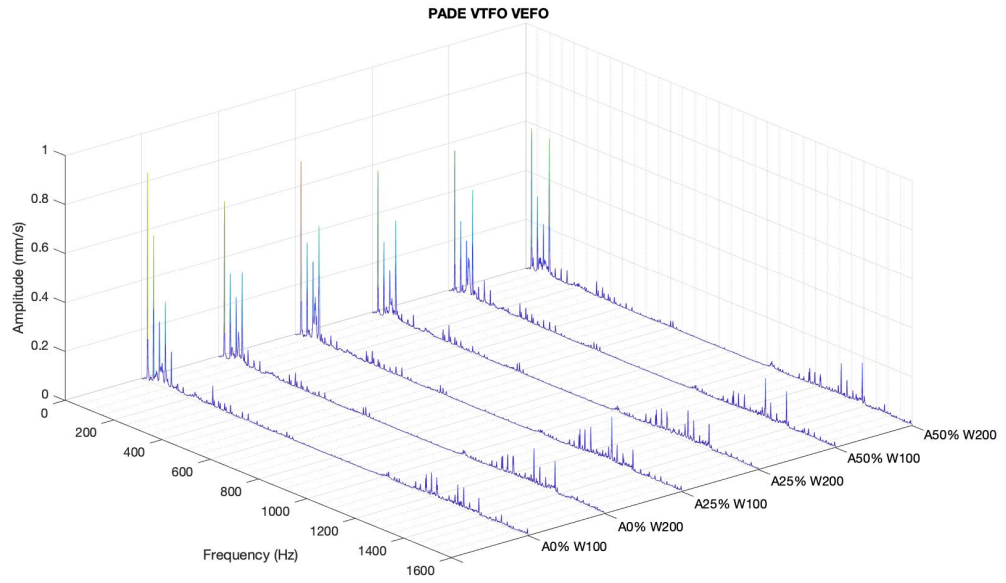


FIGURE 4.5. Graph of horizontal motor spectrum for overall flow (a) driven end (DE) (b) Non-driven end (NDE)

TABLE 4.5. Axial pump spectrum

Trial	DE		NDE	
	Max. Amplitude (mm/s)	Max. Frequency (Hz)	Max. Amplitude (mm/s)	Max. Frequency (Hz)
1	0.8496	24-25	1.8146	24-25
2	0.64387	24-25	1.491	24-25
3	0.71672	24-25	1.4805	24-25
4	0.58882	24-25	1.4784	24-25
5	0.58026	24-25	1.4938	24-25
6	0.58096	24-25	1.5074	24-25

(a)



(b)

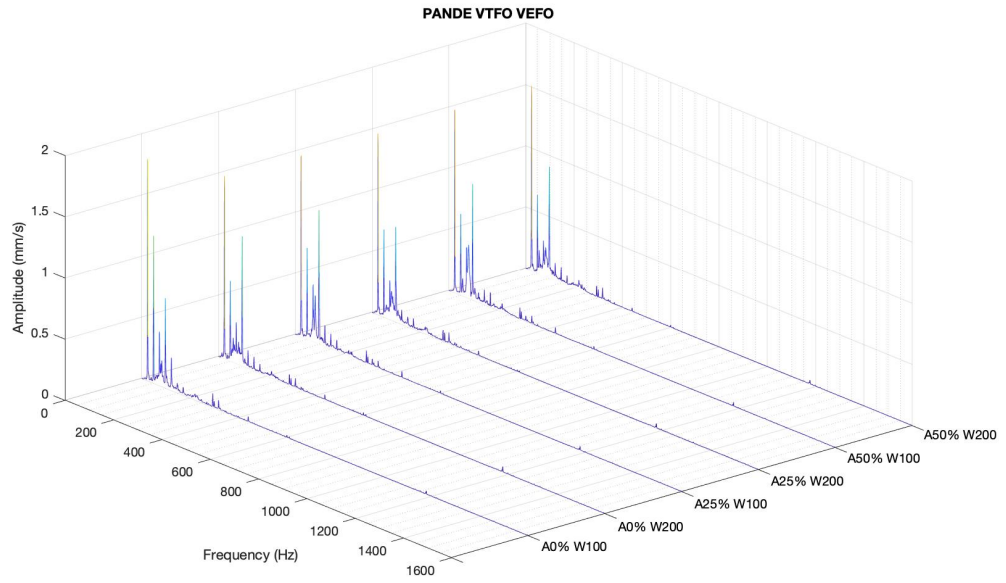
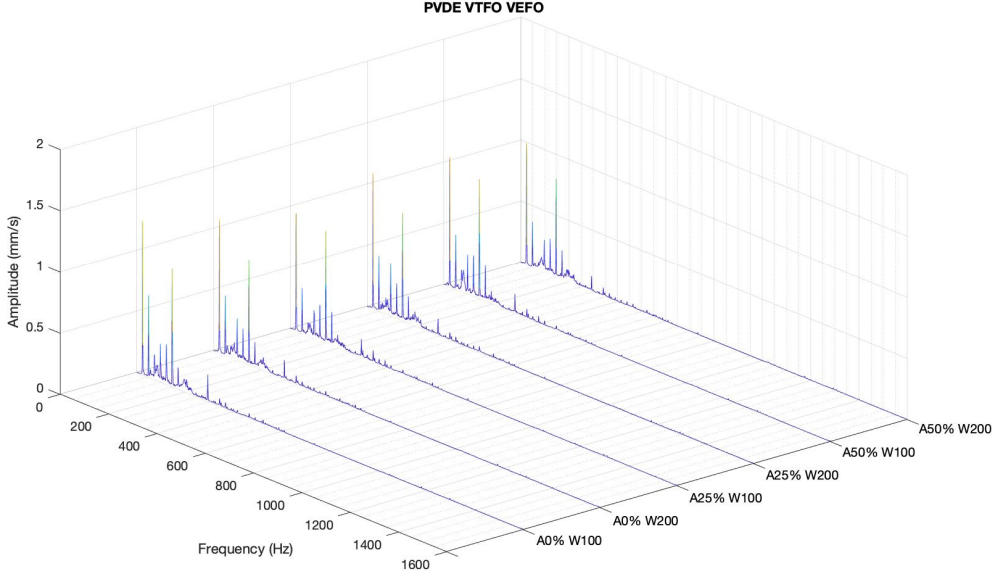


Figure 4.6. Graph of axial pump spectrum for overall flow (a) driven end (DE)
(b) Non-driven end (NDE)

TABLE 4.6. Vertical pump spectrum

Trial	DE		NDE	
	Max. Amplitude (mm/s)	Max. Frequency (Hz)	Max. Amplitude (mm/s)	Max. Frequency (Hz)
1	1.2583	98	0.8425	147
2	1.0924	98	0.79707	147
3	0.9585	98	0.90414	147
4	1.1071	98	1.0865	147
5	1.0567	98	0.91103	147
6	0.99181	98	0.78241	147

(a)



(b)

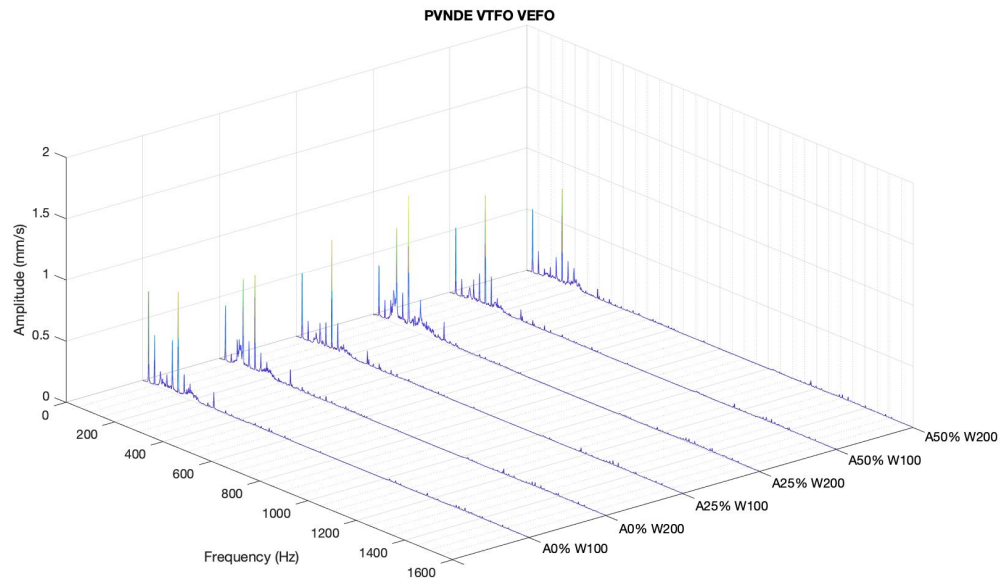
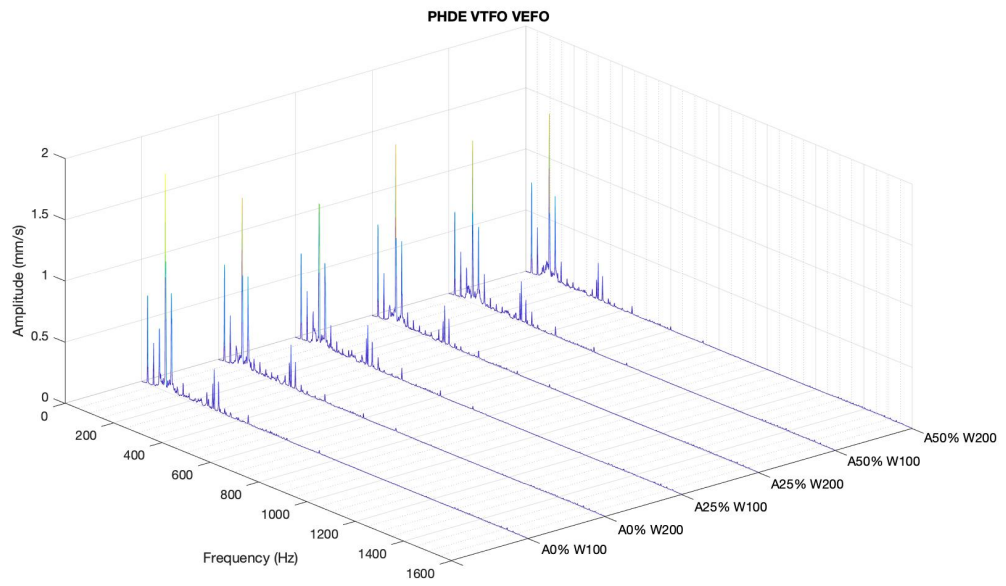


FIGURE 4.7. Graph of vertical pump spectrum for overall flow (a) driven end (DE)
(b) Non-driven end (NDE)

TABLE 4.7. Horizontal pump spectrum

Trial	DE		NDE	
	Max. Amplitude (mm/s)	Max. Frequency (Hz)	Max. Amplitude (mm/s)	Max. Frequency (Hz)
1	1.7761	98	1.3648	98
2	1.3963	98	1.2225	98
3	1.1717	98	1.0555	98
4	1.475	98	1.1253	98
5	1.3253	98	1.0539	98
6	1.3644	98	1.1057	98

(a)



(b)

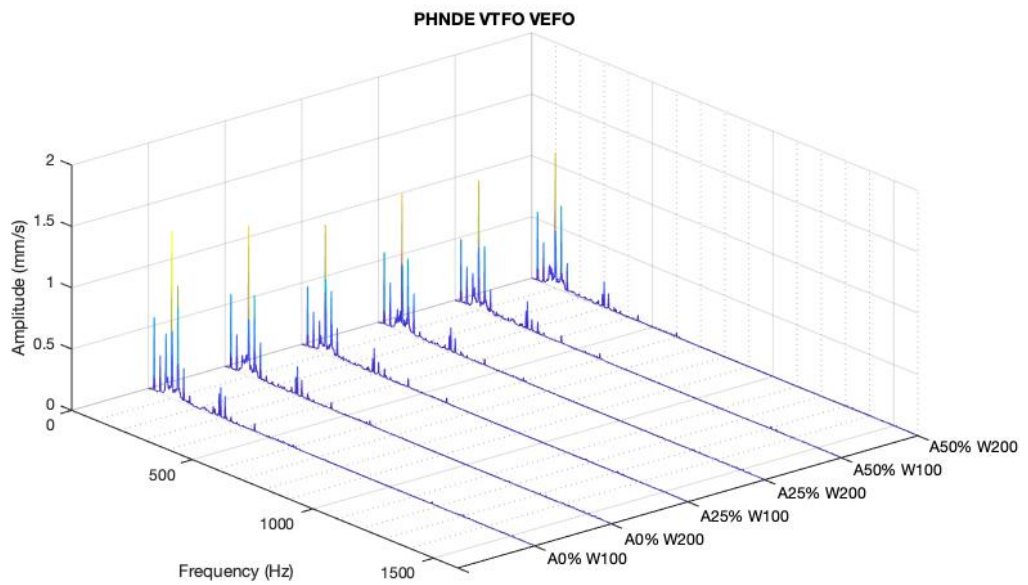
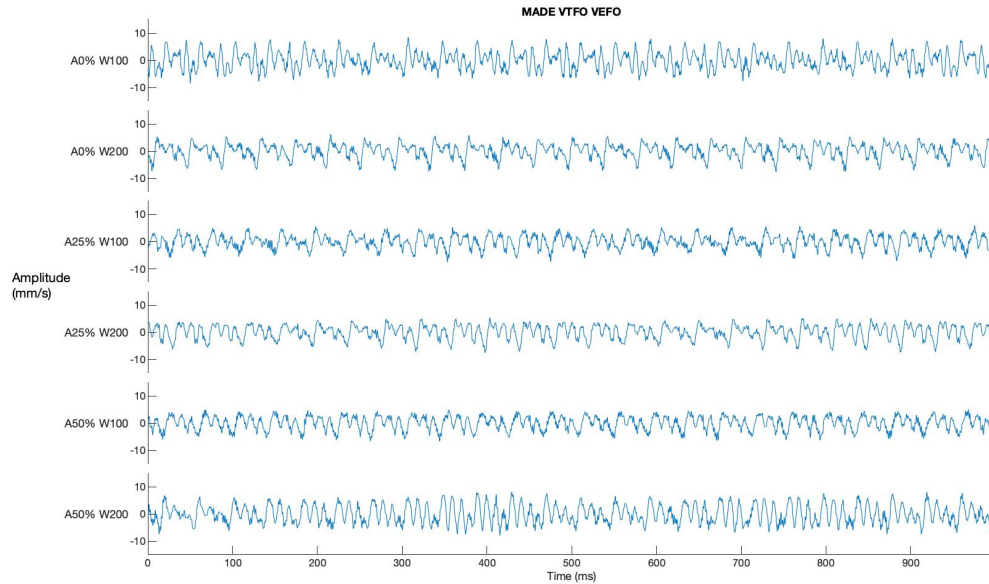


FIGURE 4.8. Graph of horizontal pump spectrum for overall flow (a) driven end (DE) (b) Non-driven end (NDE)

4.1.2 Time waveform vibration analysis

The results for motor are shown in Figure 4.9 until Figure 4.11. Meanwhile, the results for pump are shown in Figure 4.12 until Figure 4.14.

(a)



(b)

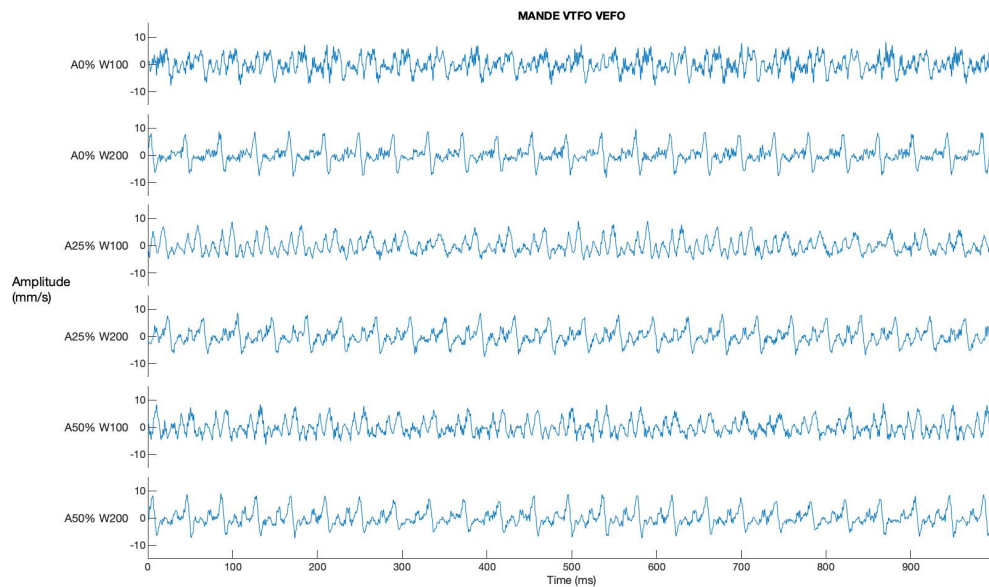
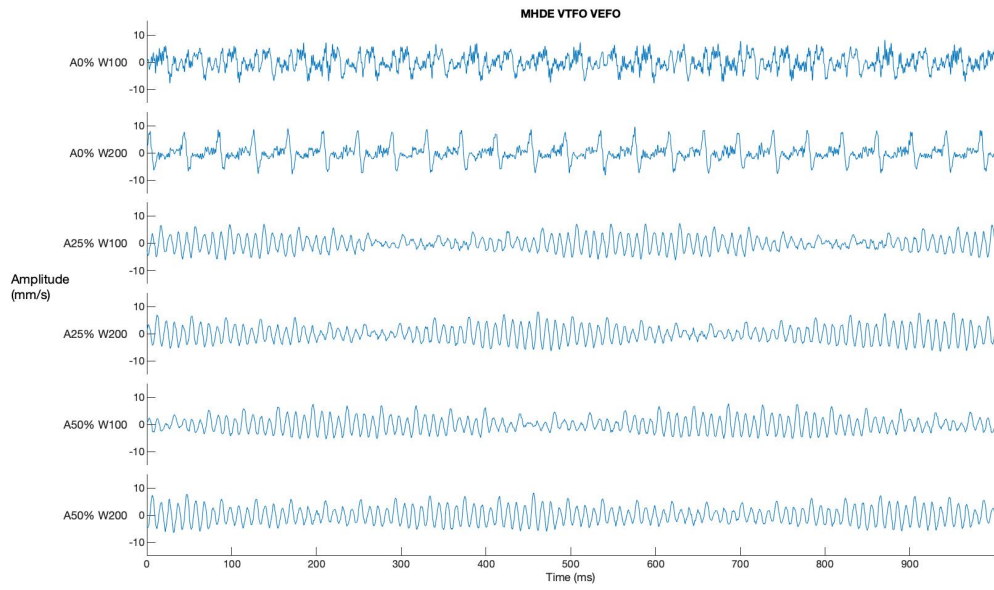


FIGURE 4.9. Graph of axial motor waveform (a) driven end (DE)
(b) Non-driven end (NDE)

(a)



(b)

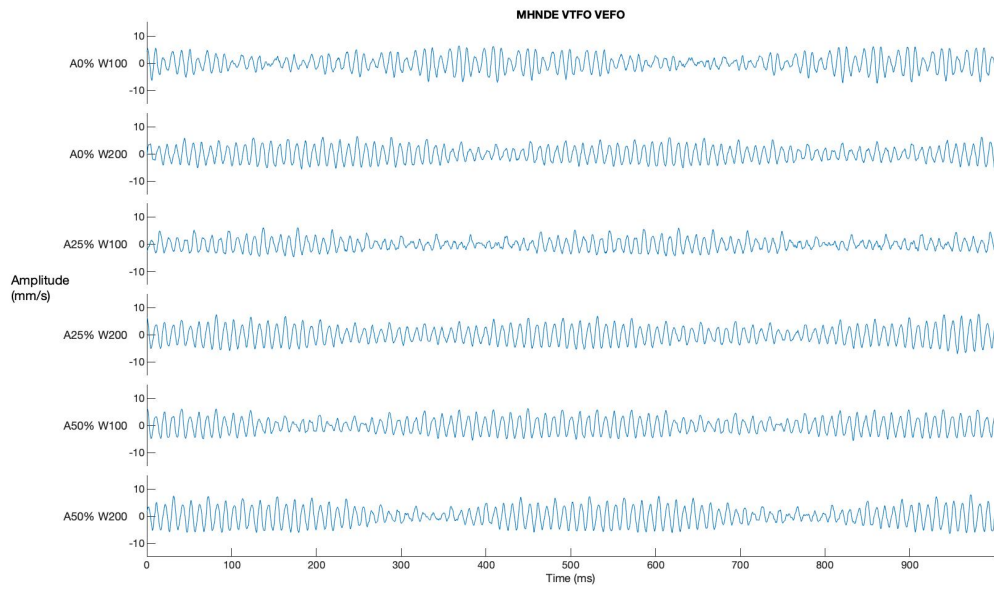
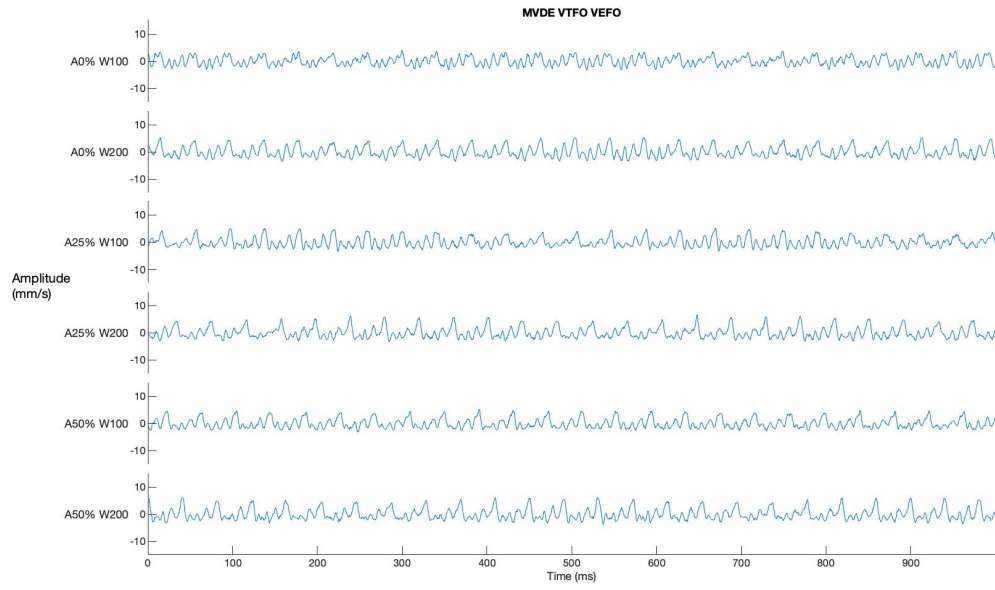


FIGURE 4.10. Graph of horizontal motor waveform (a) driven end (DE)
(b) Non-driven end (NDE)

(a)



(b)

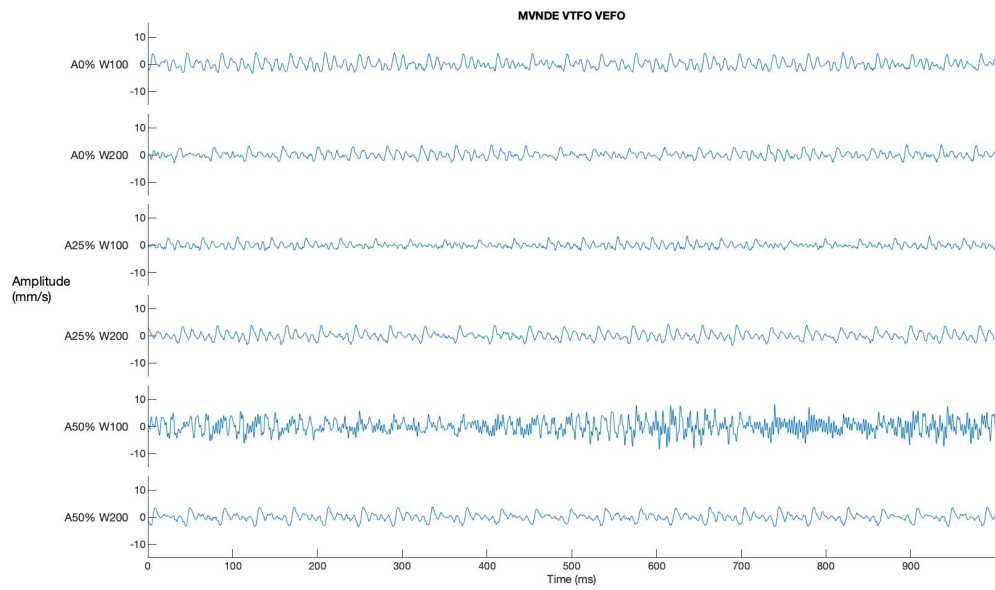
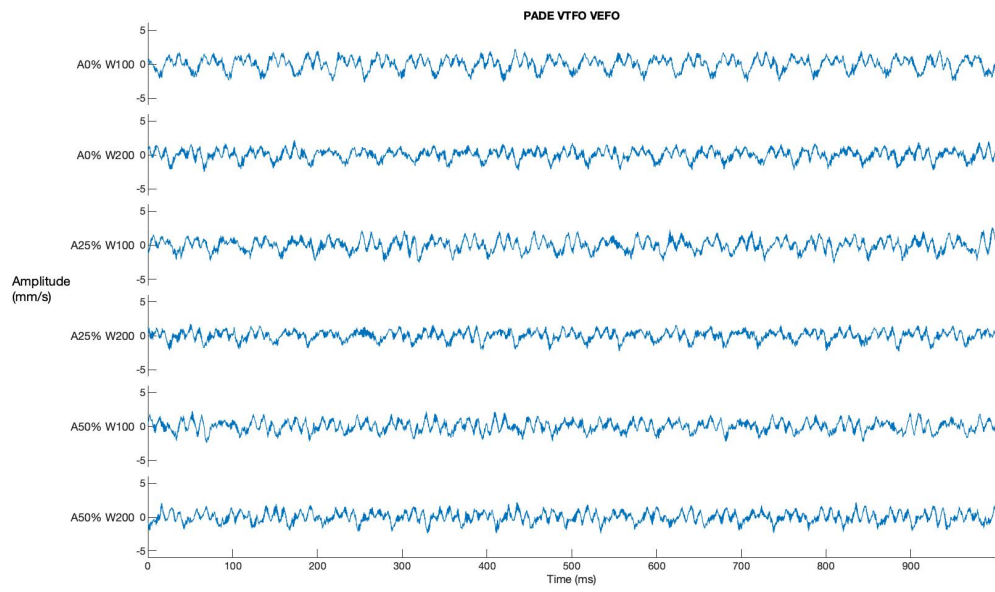


FIGURE 4.11. Graph of vertical motor waveform (a) driven end (DE)
(b) Non-driven end (NDE)

(a)



(b)

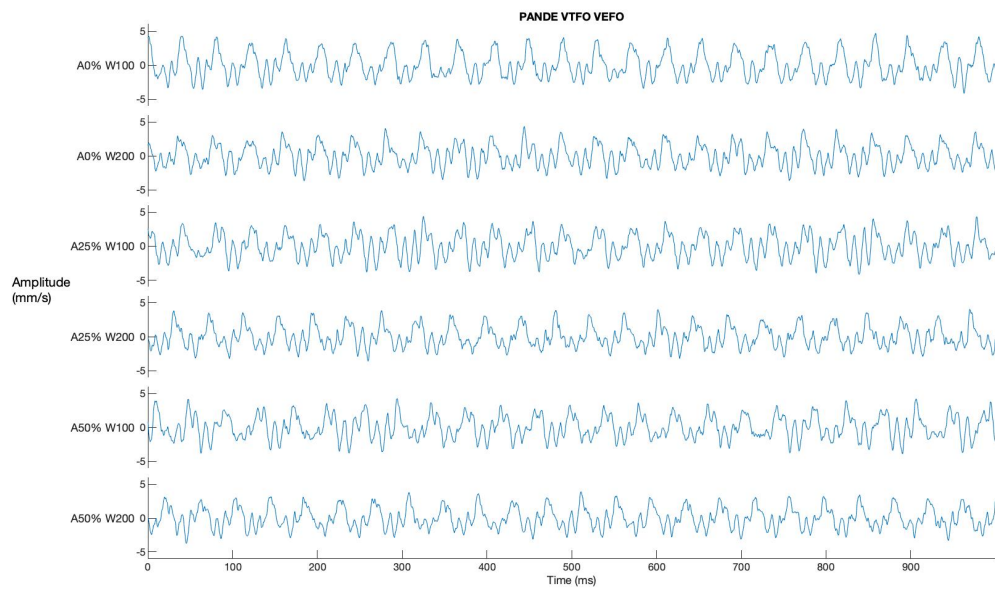
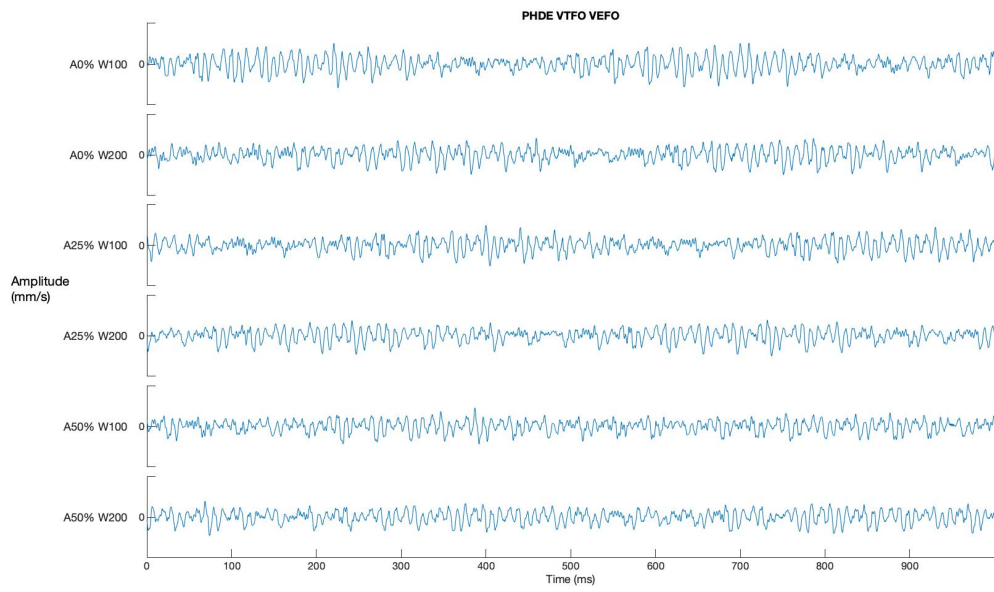


FIGURE 4.12. Graph of axial pump waveform (a) driven end (DE)
(b) Non-driven end (NDE)

(a)



(b)

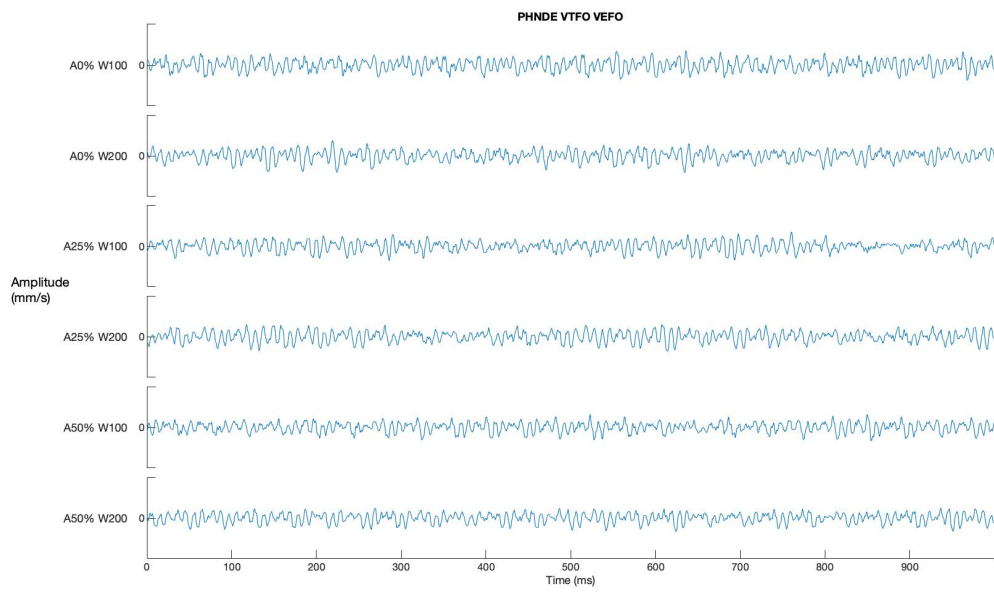
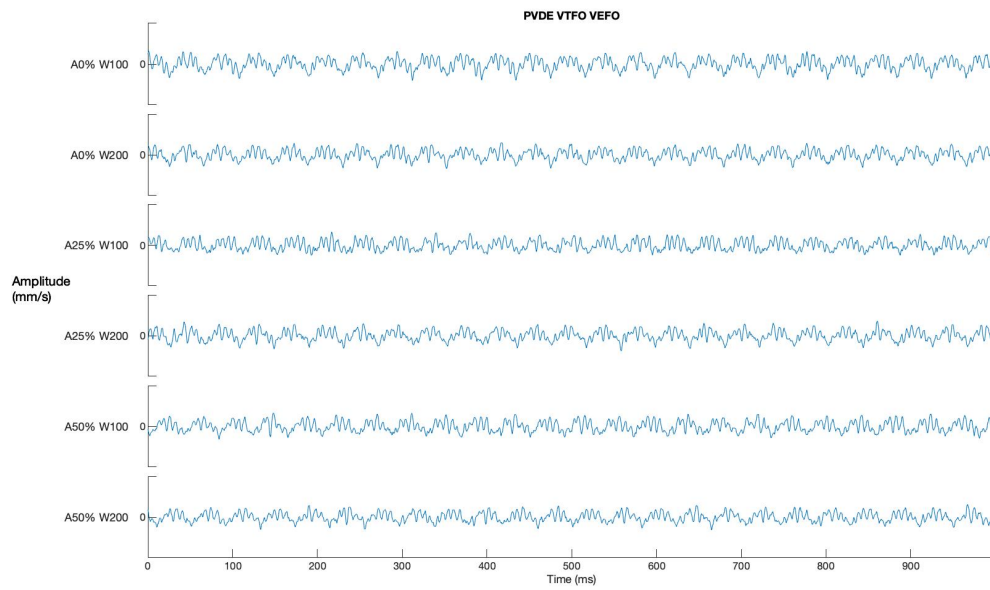


FIGURE 4.13. Graph of horizontal pump waveform (a) driven end (DE)
(b) Non-driven end (NDE)

(a)



(b)

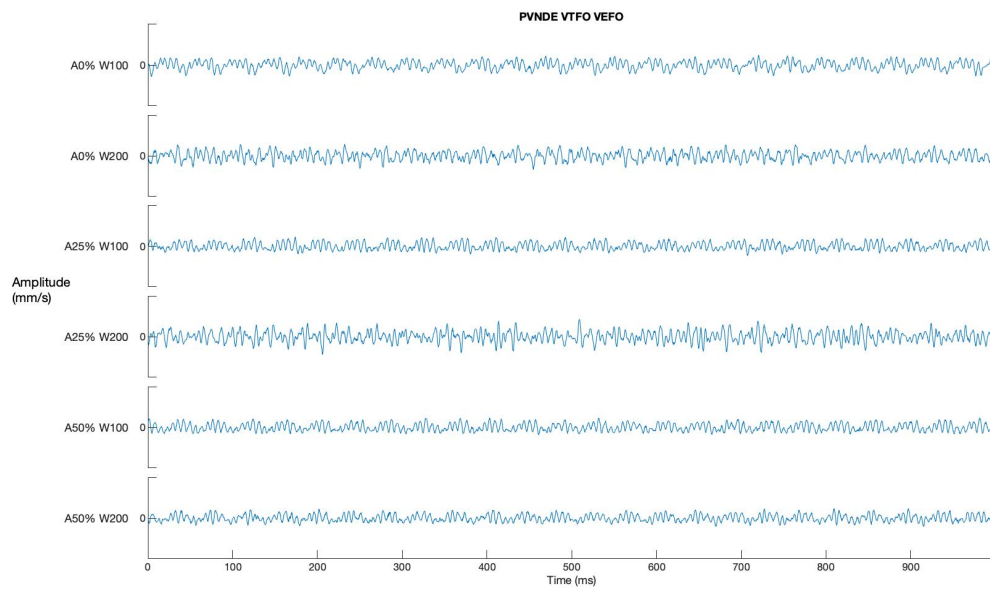


FIGURE 4.14 Graph of vertical pump waveform (a) driven end (DE)
(b) Non-driven end (NDE)

Based on the results above, we could see that the trends and patterns of the spectrum and time waveform at different void fraction values of 0%, 25% and 50% shown almost similar results. It could be observed that void fraction did not bring much effect to the mechanical induced vibration. Instead, the spectrum and time waveform pattern

has shown potential issues of the machine, which might transmit induced vibration onto the piping system.

In every position of motor-pump at different trials, the pattern shows high-frequency noise at broadband frequency spectrum around 10x until 30x. This random and “hump” shaped inside the vibration spectrum indicates the cavitation issue of motor-pump. Peak amplitude at 3x and 4x could also be seen in a certain direction at the driven end (DE) and non-driven end (NDE) motor and pump. This behavior shows a similar pattern with the misalignment issue. In general, most misalignment cases are a combination of parallel and angular misalignment. Diagnosis of this condition is based upon the dominant vibration at twice the rotational rate (4x) with increased rotational rate (3x) levels acting in the axial and either one of the radials (vertical and horizontal) directions. However, phase relationships have a great role in determining this problem. In our case, this issue cannot be concluded yet due to the unavailable datasheet and information regarding the phase. Thus, it needs to be verified further.

4.2. Effects of flow

This sub-section will discuss further the effect of vibration during flow at piping components of tee-junction and elbows by looking at the spectrum and time waveform vibration analysis and observations during the experiment.

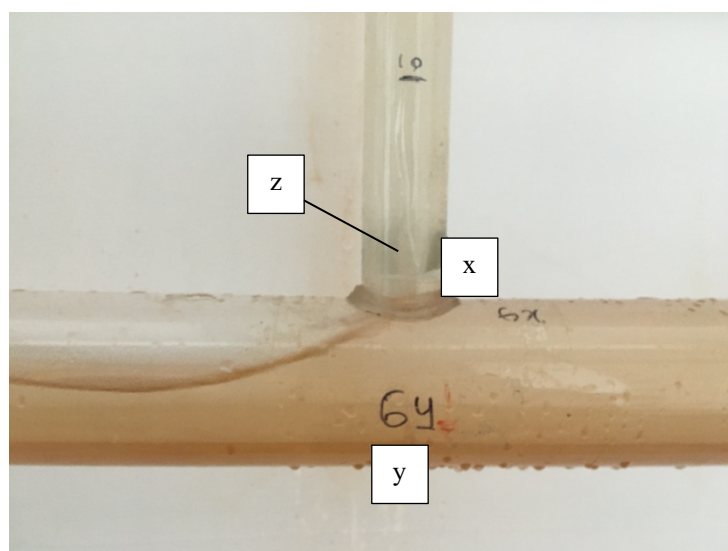


FIGURE 4.15. Tee junction (Point 6)

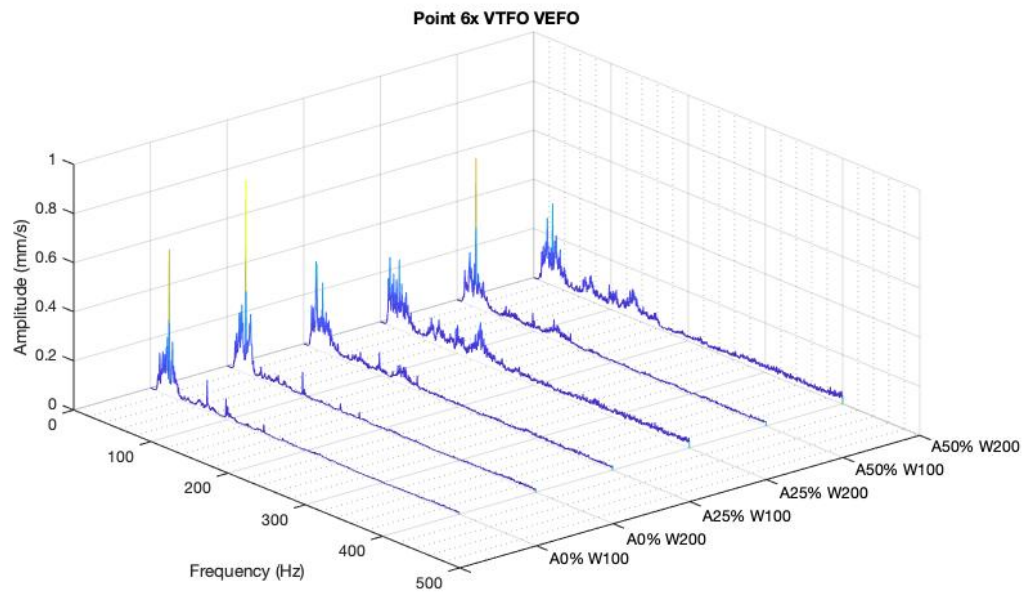
4.2.1. Point 6 (Tee junction)

The spectrum readings for point 6 are shown in Table 4.8 and Figure 4.16. Meanwhile, the time waveform reading are shown in Figure 4.17.

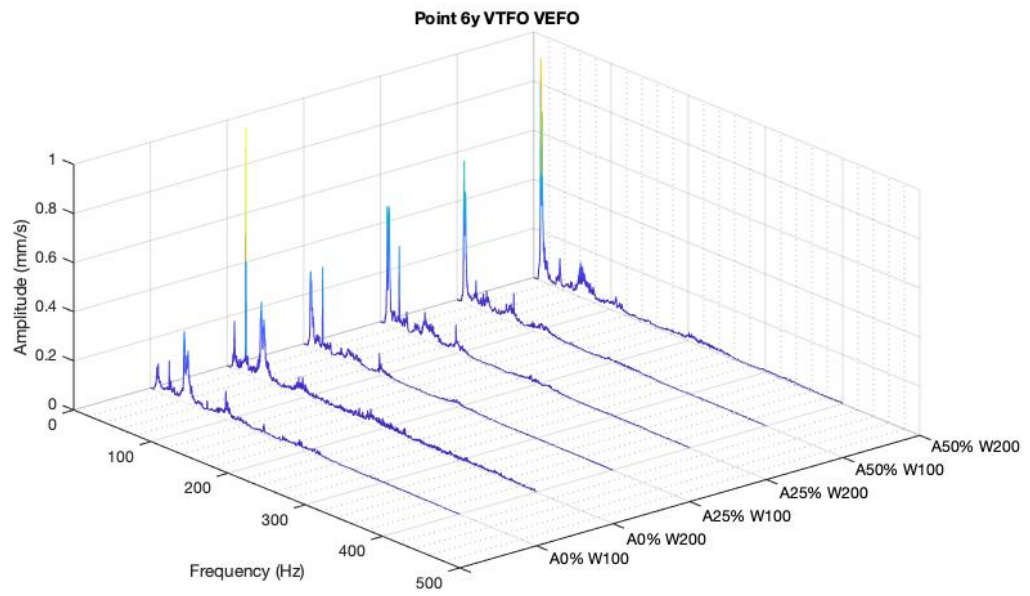
TABLE 4.8. Spectrum point 6

Trial	Point 6					
	X		y		z	
	Max. Amplitude (mm/s)	Max. Frequency (Hz)	Max. Amplitude (mm/s)	Max. Frequency (Hz)	Max. Amplitude (mm/s)	Max. Frequency (Hz)
1	0.59542	24.5	0.28736	24.5	0.65851	24.5
2	0.78751	24.5	1.0245	24.5	3.7047	24.5
3	0.35692	16.75	0.6867	11	0.35692	24.5
4	0.28424	24.5	0.53864	96.75	0.28424	24.5
5	0.60917	24.5	0.48594	11.75	0.60917	24.5
6	0.33239	24.5	0.46071	27.5	0.33239	24.5

(a)



(b)



(c)

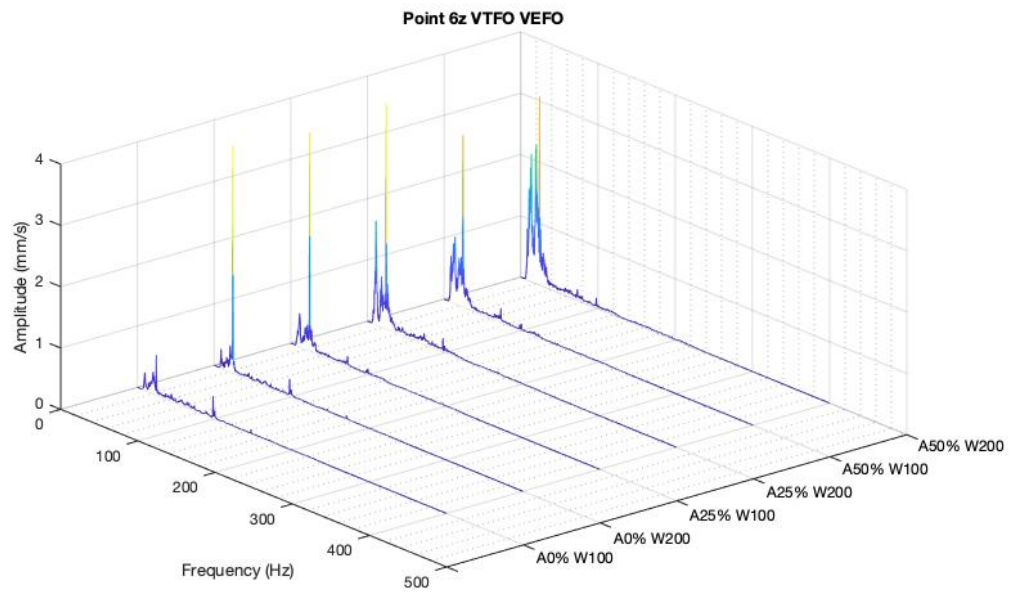
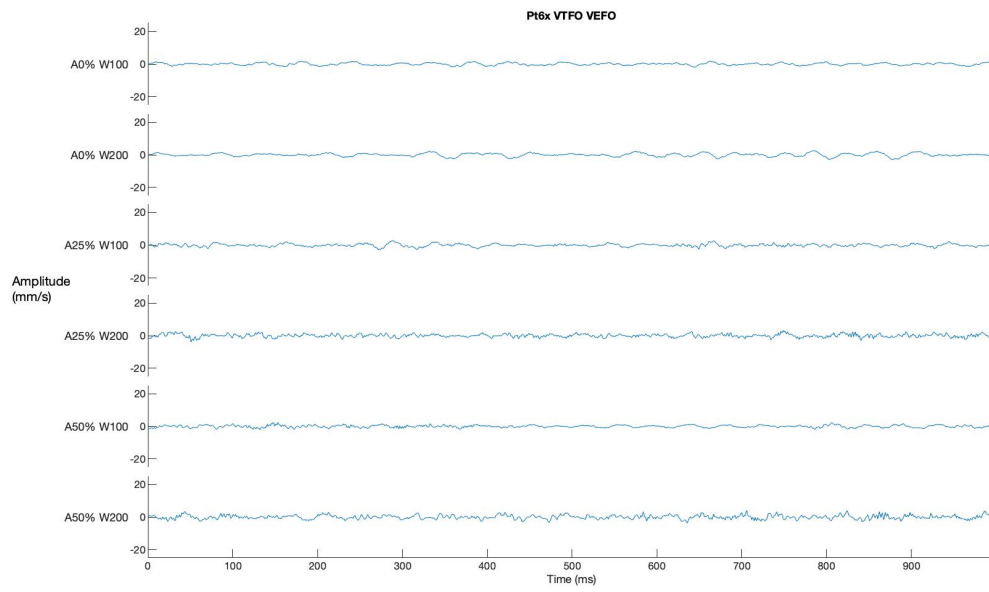
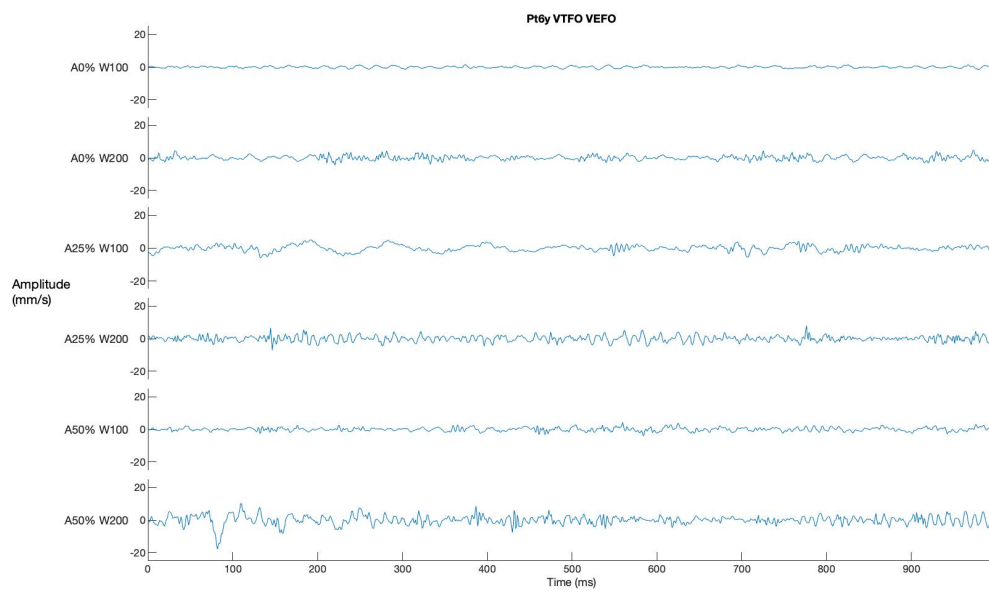


FIGURE 4.16. Graph of all flow conditions (a) Point 6x (b) Point 6y (c) Point 6z

(a)



(b)



(c)

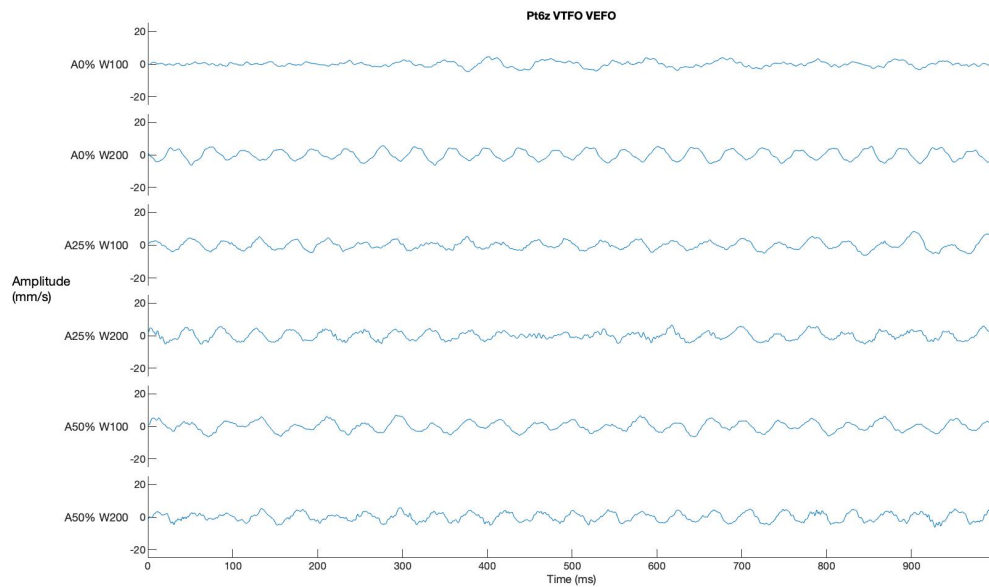
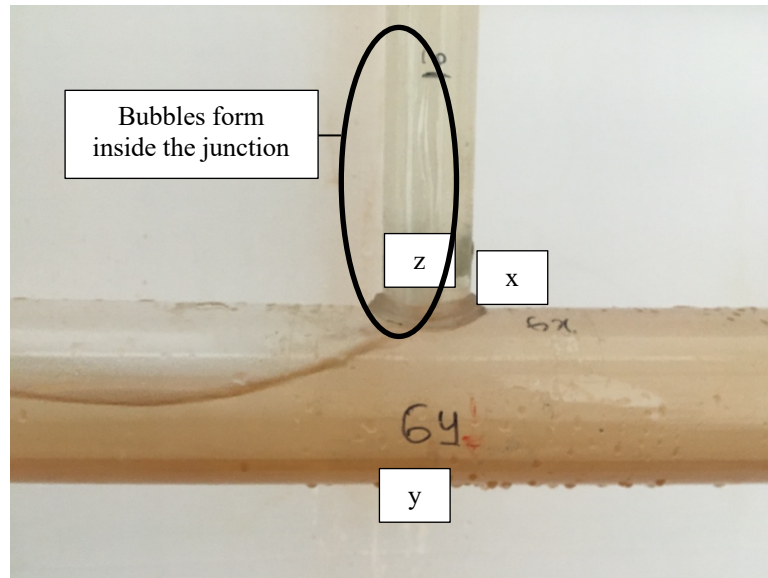


FIGURE 4.17. Graph time waveform of all flow conditions (a) Point 6x (b) Point 6y (c) Point 6z

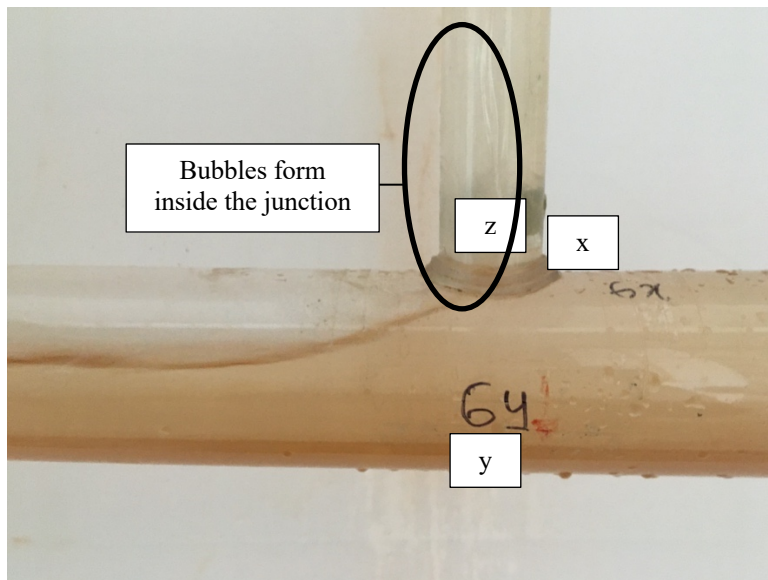
When comparing the vibration amplitude of different void fractions, it is observed that as void fraction, increases from 0%, 25% to 50%, the vibration amplitude increases slightly. Lower amplitude is seen inside the single-phase compared to the two-phase. From the results, the highest amplitude readings are observed in the z-axis with the peak at trial 2 (single-phase, water flow rate 200 l/min). Meanwhile, the lowest amplitude readings are seen on the y-axis. As shown in Figure 4.18 below, when water flows along the tee junction, it tends to fill in the right side near the x-axis. The left space is left with air and bubble. The presence of these bubbles will introduce fluctuation due to the formation and breakdown of them inside the flow. This will then generate excitation forces inside the system. Similar to the findings by Riverin and Pettigrew [23], fluctuating forces will be generated due to the variations of bubbles and droplets of various sizes through the piping system. This phenomenon explains the high amplitude readings in the z-axis as, during the formation and breakdown of bubbles, they hit the side. It is also observed that more bubbles were formed as the void fraction is increased. However, further study should be done in determining the effects of bubble sizes with the vibration level as some studies mentioned that the size of bubbles could affect the nature of the two-phase flow.

In most axis at each trial, the maximum amplitude is seen at harmonic 1x (frequency 24.5 Hz). This is due to the excitation force transmitted from the machine throughout the system. It will induced flow turbulence as shown in the sub-synchronous region and the presence of noise throughout the broadband frequency inside all conditions. Higher broadband noise frequency could be seen inside the two-phase flow.

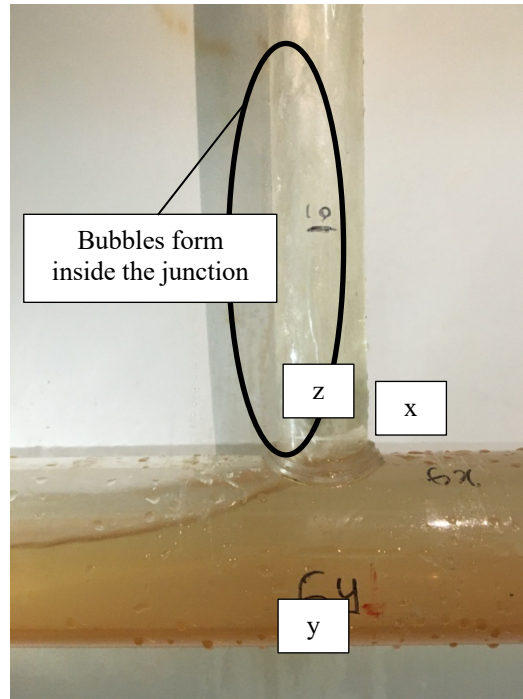
(a)



(b)



(c)



(d)

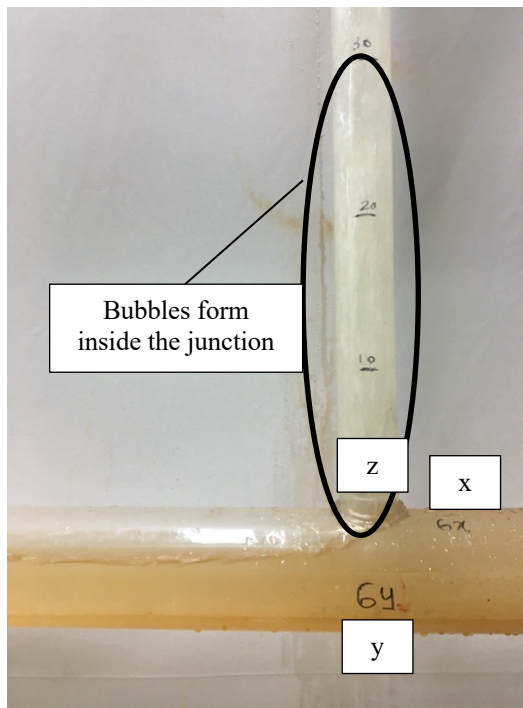


FIGURE 4.18. Bubble formation at tee-junction (Point 6) for different void fraction of (a) Trial 3 ($\beta = 25\%$, $Q_1 = 0.0017 \text{ m}^3/\text{s}$) (b) Trial 5 ($\beta = 50\%$, $Q_1 = 0.0017 \text{ m}^3/\text{s}$) (c) Trial 4 ($\beta = 25\%$, $Q_1 = 0.0033 \text{ m}^3/\text{s}$) (d) Trial 6 ($\beta = 50\%$, $Q_1 = 0.0033 \text{ m}^3/\text{s}$)

4.2.2. Point 7 (Elbow 1)

The spectrum readings for point 7 are shown in Table 4.9 and Figure 4.20. Meanwhile, the time waveform reading are shown in Figure 4.21.

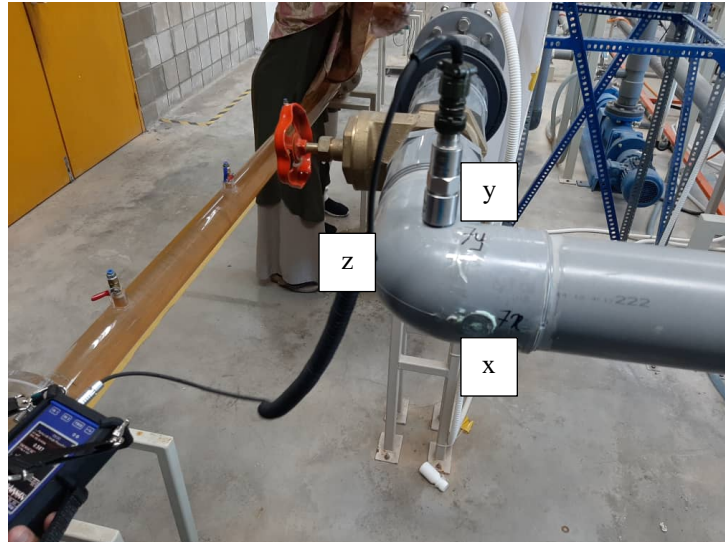
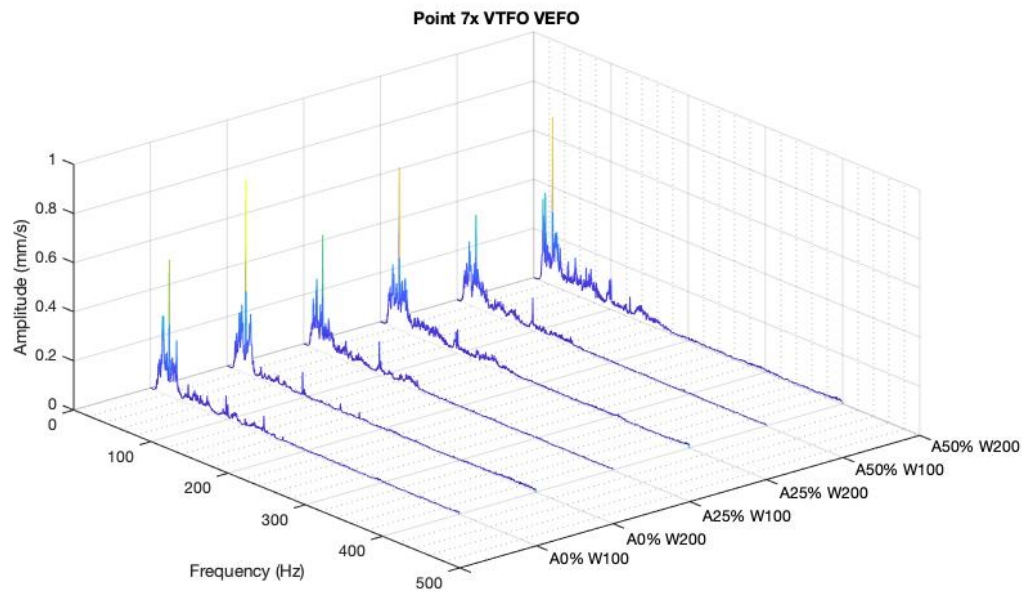


FIGURE 4.19. Elbow (Point 7)

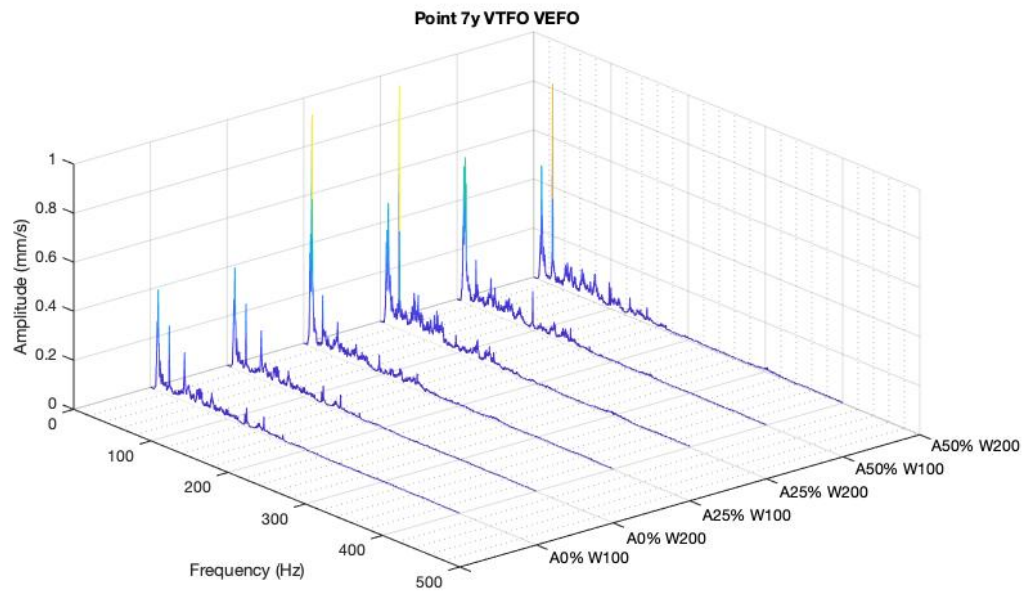
TABLE 4.9. Spectrum point 7

Trial	Point 7					
	x		y		z	
	Max. Amplitude	Max. Frequency (Hz)	Max. Amplitude	Max. Frequency (Hz)	Max. Amplitude	Max. Frequency (Hz)
1	0.5527	24.5	0.41207	10.25	0.29706	24.5
2	0.78751	24.5	0.41207	10.25	1.832	24.5
3	0.475	24.5	0.94678	10.75	0.36363	24.5
4	0.6603	24.5	0.99371	24.5	1.5615	24.5
5	0.37641	24.5	0.5926	10.75	0.31743	24.5
6	0.68402	24.5	0.81985	24.5	1.1001	24.5

(a)



(b)



(c)

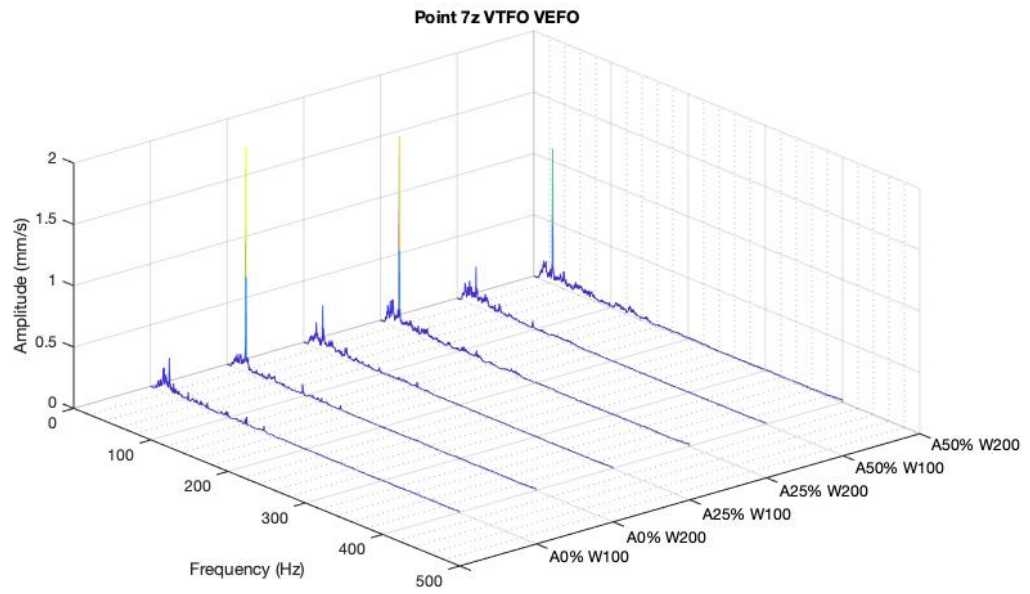
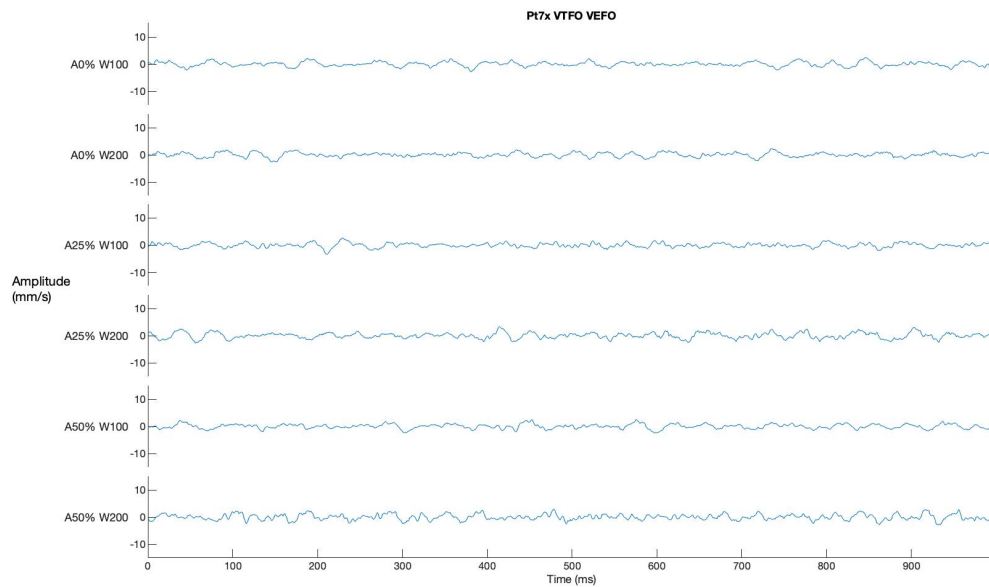
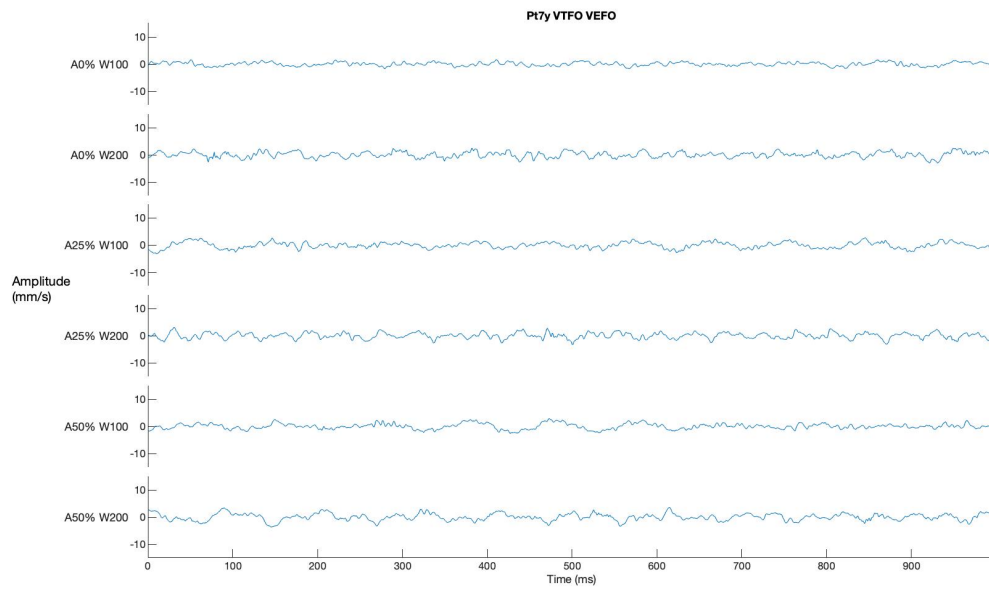


FIGURE 4.20. Graph of all flow conditions (a) Point 7x (b) Point 7y (c) Point 7z

(a)



(b)



(c)

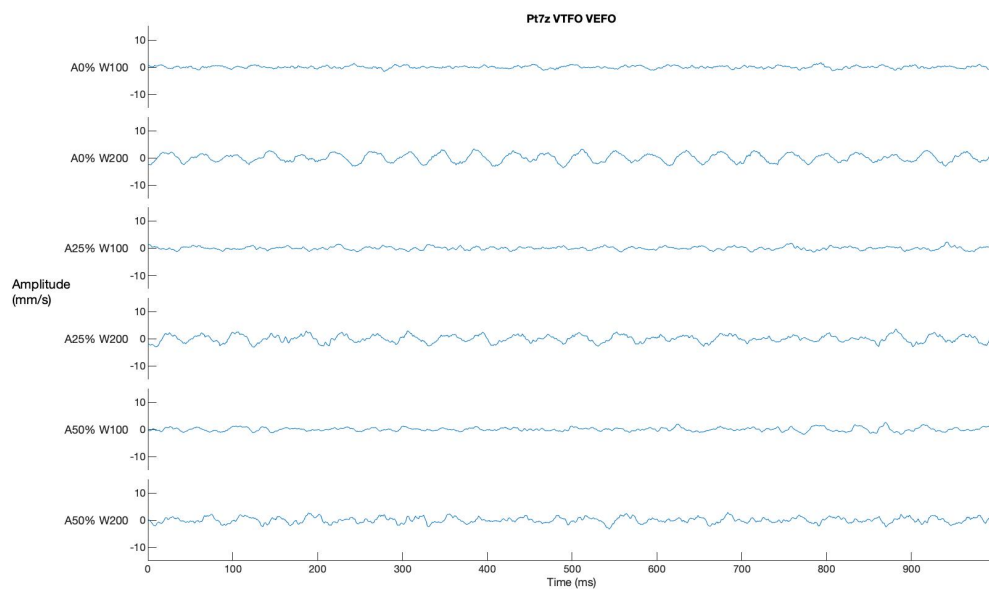


FIGURE 4.21. Graph time waveform of all flow conditions (a) Point 7x
(b) Point 7y (c) Point 7z

Based on the results, there are almost similar pattern and trends observed inside every axis as the void fraction increase. However, the amplitude inside the single-phase flow is much lower compared to the two-phase flow. This shows that there are no significant force and pressure fluctuations inside single-phase flow as explained by

Liu et. al [26] in their study. When comparing the vibration amplitude in x, y and z-axis, the highest amplitude readings could be seen at the y-axis while the lower amplitude is observed at the z-axis. Higher amplitude reading is observed at the y-axis probably due to the high impact from the backflow as the water hits the elbow. Turbulence and vortex shedding might happen in this area which may lead to water hammering. However, further validation is required in this matter as it could not be seen clearly from the spectrum and time waveform graph.

Similar to the y-axis, higher amplitude is also observed on the x-axis. This is due to the water hammering which produces impact at the elbow. There are no significant force fluctuations at z-axis as it is parallel to the water flow. Flow turbulence is also seen inside the sub-synchronous region and inside the broadband frequency area after harmonic peak 1x. This flow noises are much visible in the sub-synchronous region, probably due to the vibration transmitted by the motor and pump. It is also affected by the presence of the bubbles inside the two-phase flow as the void fraction increase. Riverin and Pettigrew [23] in their study had also found that as bubbles and droplets of various sizes from different void fraction flow through the piping elements such as elbow, it will produce fluctuation forces.

4.2.3. Point 8 (Elbow 2)

The spectrum readings for point 6 are shown in Table 4.10 and Figure 4.23. Meanwhile, the time waveform reading are shown in Figure 4.24.

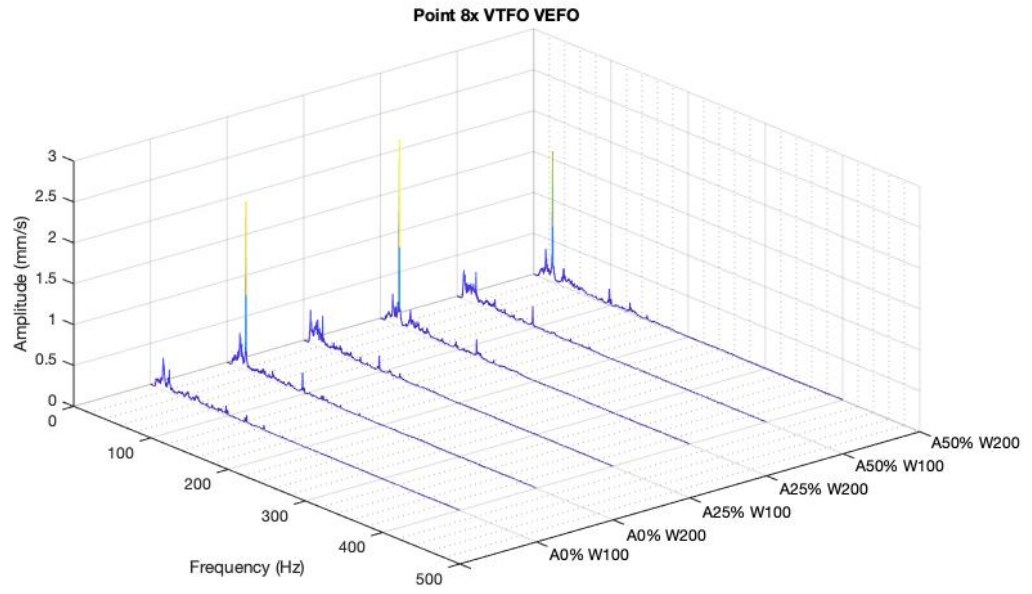


FIGURE 4.22. Elbow (Point 8)

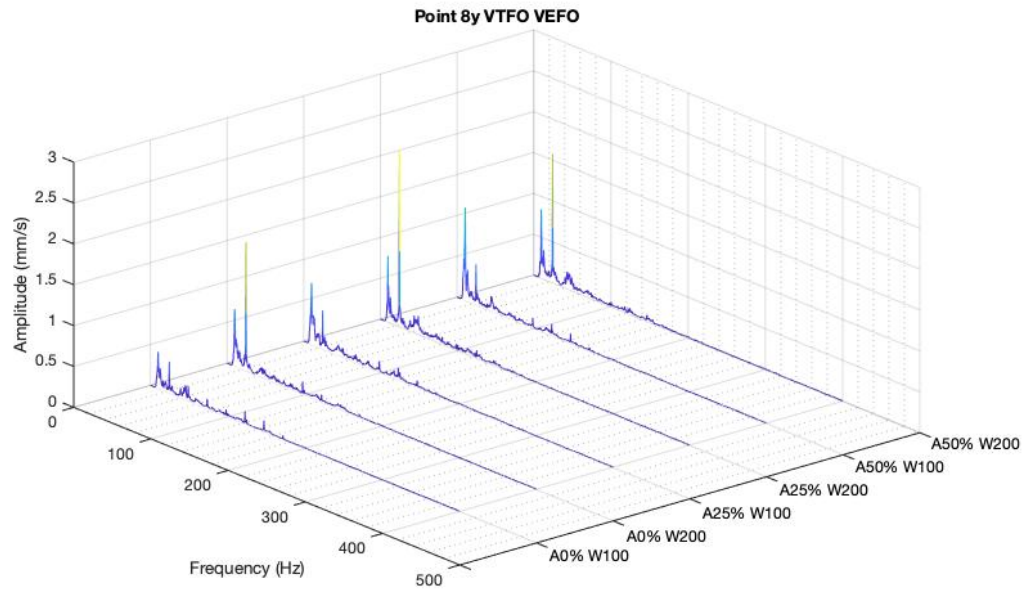
TABLE 4.10. Spectrum point 8

Trial	Point 8					
	X		y		z	
	Max. Amplitude	Max. Frequency (Hz)	Max. Amplitude	Max. Frequency (Hz)	Max. Amplitude	Max. Frequency (Hz)
1	0.3882	16.5	0.44806	10.0	0.14354	22.25
2	2.0619	24.5	1.5749	24.5	1.9015	24.5
3	0.40608	10.25	0.74964	10.5	0.73047	24.5
4	2.2845	24.5	2.164	24.5	1.0943	24.5
5	0.39	9.5	1.1371	10.5	0.79131	24.5
6	1.5995	24.5	1.5753	24.5	1.2409	24.5

(a)



(b)



(c)

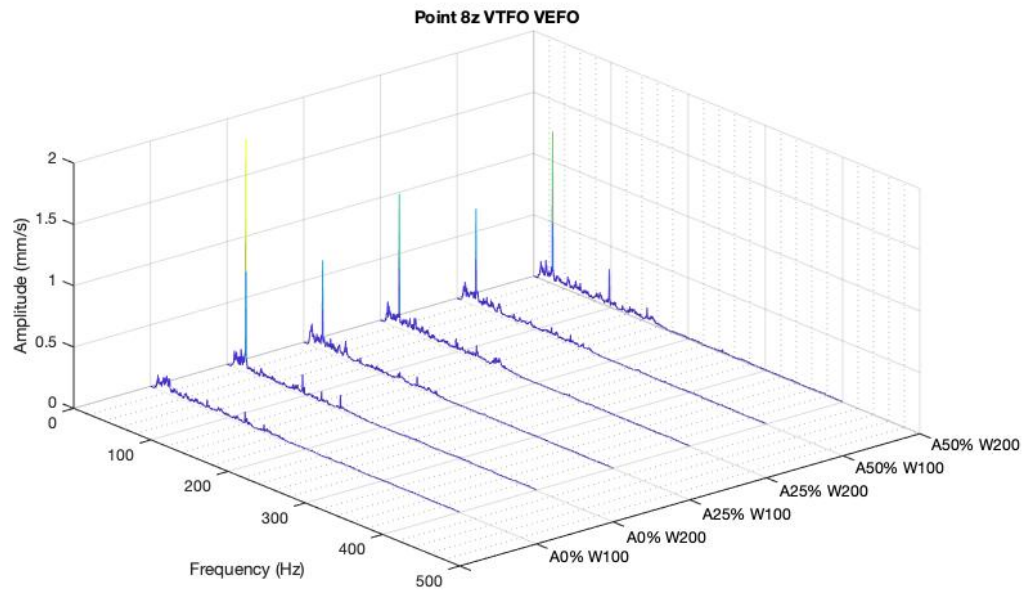
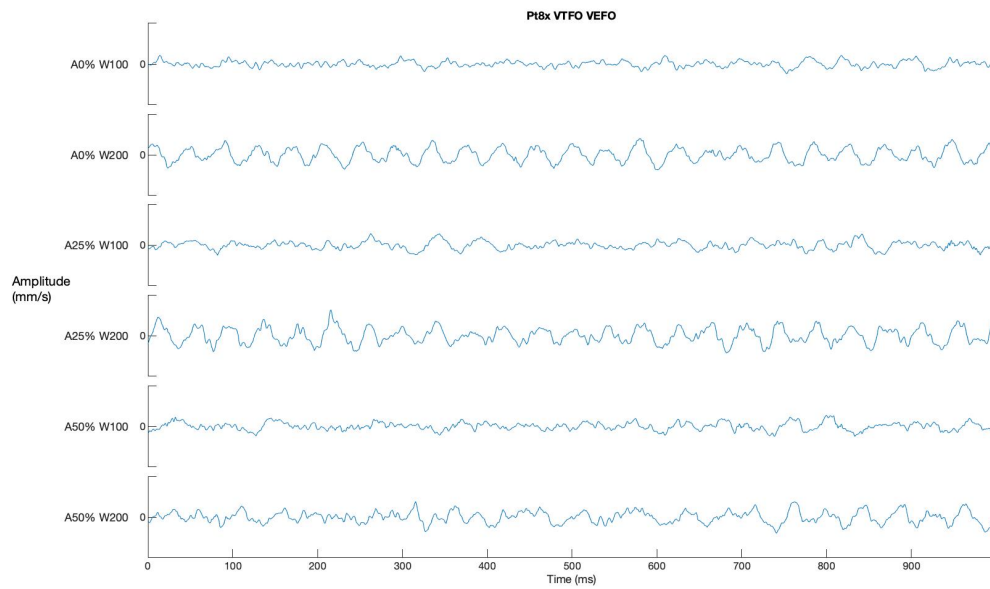
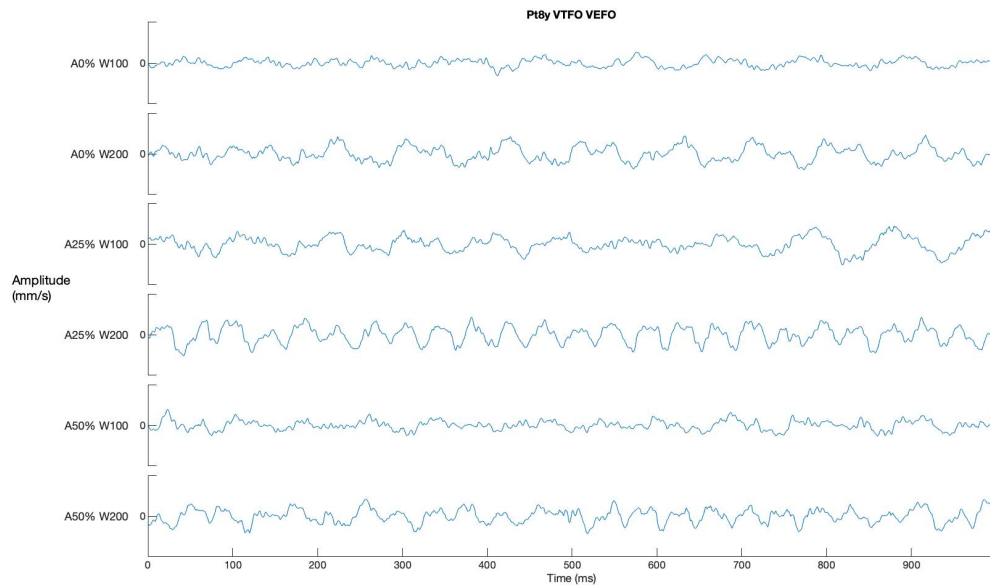


FIGURE 4.23. Graph of all flow conditions (a) Point 8x (b) Point 8y (c) Point 8z

(a)



(b)



(c)

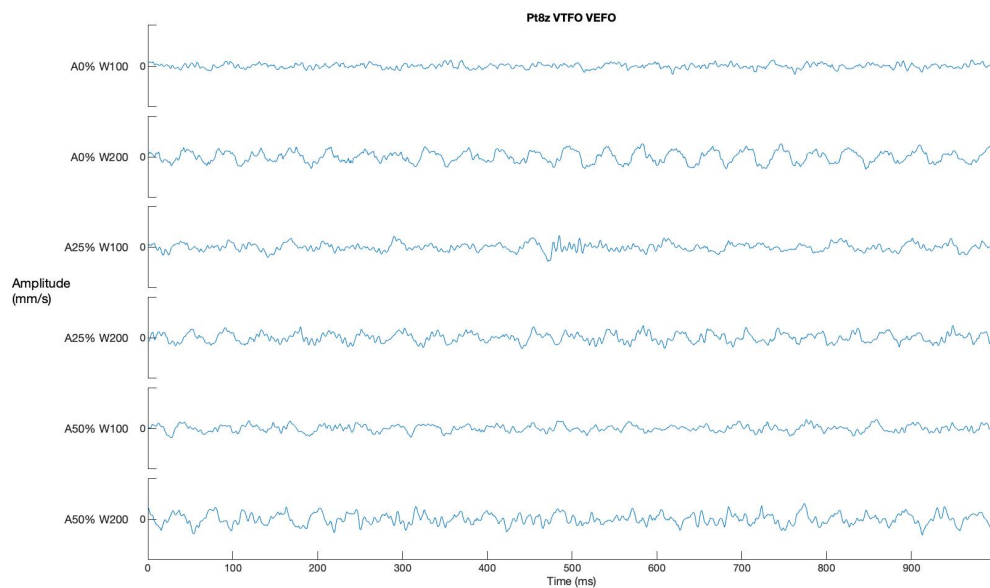


FIGURE 4.24. Graph time waveform of all flow conditions (a) Point 8x (b) Point 8y (c) Point 8z

For point 8, it could be observed that higher amplitude readings are seen at the z-axis and lower amplitude readings are seen at the x-axis. Inside the z-axis, there is no noticeable turbulence flow as the water flow is parallel to the axis, producing lower amplitude readings. In the z-axis, the incoming water flows directly onto the axis,

making a high amplitude to be observed at that position. A similar pattern might be observed at point 7. However, the position of the sensor is not directly parallel to the incoming flow. This could somehow affect the vibration amplitude reading at this axis.

There are not many differences observed from the differences of void fraction. In all conditions at x, y, and z-axis, it is observed that amplitude inside the single phase is slightly lower than two-phase. A peak at harmonic 1x could be observed in almost every condition, due to the vibration transmitted from the machine. In addition, flow turbulence is observed inside the sub-synchronous region. Visible floor noise is also observed at the broadband frequency. In comparison to point 7, vibration amplitude at point 8 is much higher due to the short distance between points 7 and 8. As the water flows into point 7 and hits the elbow, the water becomes much unstable. The incoming unstable flow will induce much higher fluctuation, producing higher vibration at point 8.

CHAPTER 5

CONCLUSION AND RECOMMENDATION

In conclusion, as shown in Figure 5.1 below, the slug flow pattern could be observed clearly during the experiment at two-phase flow as the void fraction increase. As stated by Riverin and Pettigrew [23], slug flow comprises of regular impulses force of the liquid. It is also cross-checked against established flow-regime map and its corresponding equations Based on the analyse done for the motor and pump in this experiment, the major problems that the motor-pump have are cavitation and misalignment. This could instigate an excitation mechanism onto the piping system and produced vibration.

From the results obtained, there is a slight effect of increasing void fraction into the piping vibration. Results obtained for the two-phase flow show higher vibration amplitude than single-phase flow. The increment of void fraction, $\beta = 0\%$, 25% , and 50% also displayed an increment in the amplitude readings. This induced a high vibration which had to affect the piping system especially at piping elements such as tee-junction and elbow. As being analysed by Wachel et. al [4], turbulence or flow-induced pulsation might be produced when flow passes through an obstruction. This will then produce noise and vibration onto the system. Thus, increasing the void fraction of flow will bring an effect onto the piping system.

(a)



(b)



FIGURE 5.1. Slug flow formation at tee-junction (Point 6) for different void fraction of (a) Trial 3 ($\beta = 25\%$, $Q_1 = 0.0017 \text{ m}^3/\text{s}$) (b) Trial 5 ($\beta = 50\%$, $Q_1 = 0.0017 \text{ m}^3/\text{s}$)

From this study, there are a few recommendations that could be made. Some of them include:

1. Validation and improvement of the results could be done by conducting simulation using existing software such as ANSYS.
2. Further study should be done in determining the effects of bubble sizes with the vibration level as some studies mentioned that the size of bubbles could affect the nature of the two-phase flow.

REFERENCES

- [1] H. Locharia, I. Al Awadhi, S. Narayana, A. Al Ahmad, and R. Mirandha, "Flow Induced Vibration in Multi Phase Piping Systems - Successful Mitigation," pp. 1 - 9, 2017, doi: SPE-188386-MS.
- [2] L. Zhu and Y. Jiang, "Modal analysis of liquid-filled pipeline under fluid-structure interaction by simulation and experiment methods," *Vibroengineering PROCEDIA*, vol. 21, pp. 42-47, 2018, doi: 10.21595/vp.2018.20307.
- [3] E. S. Udoetok, "Internal Fluid Flow Induced Vibration of Pipes " *Journal of Mechanical Design and Vibration* vol. 6, no. 1, pp. 1-8, 2018, doi: 10.12691/jmdv-6-1-1.
- [4] S. J. M. J. C. Wachel, Kenneth E. Atkins, "Piping Vibration Analysis."
- [5] Z. C. Ong, H. C. Eng, and S. Noroozi, "Non-destructive testing and assessment of a piping system with excessive vibration and recurrence crack issue: An industrial case study," *Engineering Failure Analysis*, vol. 82, pp. 280-297, 2017, doi: 10.1016/j.engfailanal.2016.12.007.
- [6] Y. D. Baba, A. E. Archibong, A. M. Aliyu, and A. I. Ameen, "Slug frequency in high viscosity oil-gas two-phase flow: Experiment and prediction," *Flow Measurement and Instrumentation*, vol. 54, pp. 109-123, 2017, doi: 10.1016/j.flowmeasinst.2017.01.002.
- [7] A. L. Gama, "Experimental Study on the measurement of two-phase flow rate using pipe vibration," 2009.
- [8] R. Rahimi, E. Bahramifar, and M. Mazarei Sotodeh, "The Indication of Two-Phase Flow Pattern and Slug Characteristics in a Pipeline Using CFD Method," *Gas Processing Journal*, vol. 1, no. 1, 1, pp. 70 - 87, 2012.
- [9] D. Zhao, L. Guo, X. Hu, X. Zhang, and X. Wang, "Experimental study on local characteristics of oil–water dispersed flow in a vertical pipe," *International Journal of Multiphase Flow*, vol. 32, no. 10-11, pp. 1254-1268, 2006, doi: 10.1016/j.ijmultiphaseflow.2006.06.004.
- [10] S. Z. Rouhani and M. S. Sohal, "Two-phase Flow Patterns: A Review of Research Results," *Progress in Nuclear Energy*, vol. 11, 3, 1982.
- [11] S. Miwa, M. Mori, and T. Hibiki, "Two-phase flow induced vibration in piping systems," *Progress in Nuclear Energy*, vol. 78, pp. 270-284, 2015, doi: 10.1016/j.pnucene.2014.10.003.
- [12] Deendarlianto, A. Rahmandhika, A. Widyatama, O. Dinaryanto, A. Widyaparaga, and Indarto, "Experimental study on the hydrodynamic behavior of gas-liquid air-water two-phase flow near the transition to slug flow in horizontal pipes," *International Journal of Heat and Mass Transfer*, vol. 130, pp. 187-203, 2019, doi: 10.1016/j.ijheatmasstransfer.2018.10.085.
- [13] T. Zhang, Y. O. Zhang, and H. Ouyang, "Structural vibration and fluid-borne noise induced by turbulent flow through a 90° piping elbow with/without a

- guide vane," *International Journal of Pressure Vessels and Piping*, vol. 125, pp. 66-77, 2015, doi: 10.1016/j.ijpvp.2014.09.004.
- [14] E. P. Robert, "Mass Flow Measurement Through Flow-Induced Pipe Vibration," 2004.
- [15] M. J. Pettigrew and C. E. Taylor, "Two-Phase Flow-Induced Vibration: An Overview," *Journal of Pressure Vessel Technology*, vol. 1, 1994.
- [16] M. A. Woldesemayat and A. J. Ghajar, "Comparison of void fraction correlations for different flow patterns in horizontal and upward inclined pipes," *International Journal of Multiphase Flow*, vol. 33, no. 4, pp. 347-370, 2007, doi: 10.1016/j.ijmultiphaseflow.2006.09.004.
- [17] X.-X. Xu, "Study on oil–water two-phase flow in horizontal pipelines," *Journal of Petroleum Science and Engineering*, vol. 59, no. 1-2, pp. 43-58, 2007, doi: 10.1016/j.petrol.2007.03.002.
- [18] N. Yusuf, Y. Al-Wahaibi, T. Al-Wahaibi, A. Al-Ajmi, A. S. Olawale, and I. A. Mohammed, "Effect of oil viscosity on the flow structure and pressure gradient in horizontal oil–water flow," *Chemical Engineering Research and Design*, vol. 90, no. 8, pp. 1019-1030, 2012, doi: 10.1016/j.cherd.2011.11.013.
- [19] P. Angeli and G. F. Hewitt, "Flow structure in horizontal oil-water flow," *International Journal of Multiphase Flow* 26, 1999.
- [20] A. L. Gama, L. R. d. S. Ferreira, and P. H. A. W. Filho, "Experimental study on the measurement of two-phase flow rate using pipe vibration," 2009.
- [21] M. Darzi and C. Park, "Experimental Visualization and Numerical Simulation of Liquid-gas two-phase flows in a horizontal pipe," 3-9 November 2017 2017.
- [22] Y. Zhou, H. Chang, and Y. Lv, "Gas-liquid two-phase flow in a horizontal channel under nonlinear oscillation: Flow regime, frictional pressure drop and void fraction," *Experimental Thermal and Fluid Science*, vol. 109, 2019, doi: 10.1016/j.expthermflusci.2019.109852.
- [23] J. L. Riverin and M. J. Pettigrew, "Vibration Excitation Forces Due to Two-Phase Flow in Piping Elements," *Journal of Pressure Vessel Technology*, vol. 129, no. 1, pp. 7-13, 2007, doi: 10.1115/1.2388994.
- [24] Y. Xue, H. Li, C. Hao, and C. Yao, "Investigation on the void fraction of gas–liquid two-phase flows in vertically-downward pipes," *International Communications in Heat and Mass Transfer*, vol. 77, pp. 1-8, 2016, doi: 10.1016/j.icheatmasstransfer.2016.06.009.
- [25] L. E. Ortiz-Vidal, N. W. Mureithi, and O. M. H. Rodriguez, "Vibration response of a pipe subjected to two-phase flow: Analytical formulations and experiments," *Nuclear Engineering and Design*, vol. 313, pp. 214-224, 2017, doi: 10.1016/j.nucengdes.2016.12.020.
- [26] Y. Liu *et al.*, "Experimental study of internal two-phase flow induced fluctuating force on a 90° elbow," *Chemical Engineering Science*, vol. 76, pp. 173-187, 2012, doi: 10.1016/j.ces.2012.04.021.